https://doi.org/10.5194/bg-2021-63
Preprint. Discussion started: 16 March 2021

Biogeosciences Discussions
Open Access
EGU

Modeling the interinfluence of fertilizer-induced NH_3 emission, nitrogen deposition, and aerosol radiative effects using modified CESM2

Ka Ming Fung[1,a], Maria Val Martin[2], Amos P. K. Tai[1,3]

[1] Graduate Division of Earth and Atmospheric Sciences, The Chinese University of Hong Kong, Sha Tin, Hong Kong
[2] Leverhulme Centre for Climate Change Mitigation, Department of Animal & Plant Sciences, University of Sheffield, Sheffield, UK
[3] Institute of Environment, Energy and Sustainability, and State Key Laboratory of Agrobiotechnology, The Chinese University of Hong Kong, Sha Tin, Hong Kong
[a] Now at: Department of Civil and Environmental Engineering, Massachusetts Institute of Technology, Cambridge, MA, USA

Correspondence to: Ka Ming Fung (kamingfung@mit.edu) & Amos P. K. Tai (amostai@cuhk.edu.hk)

Abstract. Global ammonia (NH_3) emission is expected to continue to rise due to intensified fertilization for growing food to satisfy the increasing demand worldwide. Previous studies focused mainly on estimating the land-to-atmosphere NH_3 injection but seldom addressed the other side of the bidirectional nitrogen exchange – deposition. Ignoring this significant input source of soil mineral nitrogen may lead to an underestimation of NH_3 emissions from natural sources. Here, we used an Earth system model to quantify NH_3-induced changes in atmospheric composition and the consequent impacts on the Earth's radiative budget and biosphere, as well as the impacts of deposition on NH_3 emissions from the land surface. We implemented a new scheme into the Community Land Model version 5 (CLM5) of the Community Earth System Model version 2 (CESM2) to estimate the volatilization of ammonium salt (NH_4^+) associated with synthetical fertilizers into gaseous NH_3. We further parameterized the amount of emitted NH_3 captured in the plant canopy to derive a more accurate quantity of NH_3 that escapes to the atmosphere. Our modified CLM5 estimated that 11 Tg-N yr^{-1} of global NH_3 emission is attributable to synthetic fertilizers. Interactively coupling terrestrial NH_3 emissions to atmospheric chemistry simulations by the Community Atmospheric Model version 4 with chemistry (CAM4-chem), we found that such emissions favor the formation and deposition of NH_4^+ aerosol, which in turn disrupts the aerosol radiative effect and enhances soil NH_3 volatilization in regions downwind of fertilized croplands. Our fully-coupled simulations showed that global-total NH_3 emission is enhanced by nitrogen deposition by 2.4 Tg-N yr^{-1}, when compared to the baseline case with 2000-level fertilization but without deposition-induced enhancements. In synergy with observations and emission inventories, our work

https://doi.org/10.5194/bg-2021-63
Preprint. Discussion started: 16 March 2021


Biogeosciences
Discussions
Open Access
EGU

provides a useful tool for stakeholders to evaluate the intertwined relations between agricultural trends, fertilize use, NH_3 emission, atmospheric aerosols, and climate, so as to derive optimal strategies for securing both food production and environmental sustainability.

1. Introduction

Global NH3 emission has risen from 59 to 65 Tg-N yr^{-1} during 2000–2008, driven mainly by the increasing fertilizer use and manure handling in farms and animal operations (Sutton et al., 2013). After entering the atmosphere, NH_3 gas readily neutralizes sulfuric acid (H_2SO_4) and nitric acid (HNO_3), which are derived from the oxidation of sulfur dioxide (SO_2) and nitrogen oxides (NO_x), forming inorganic sulfate-nitrate-ammonium (SNA) aerosols (Behera and Sharma, 2012). These ammonium ($NH4^+$) salts can constitute 25–75% of inorganic fine particulate matter ($PM_{2.5}$, particles with an aerodynamic diameter <2.5 μm) (Ianniello et al., 2011; Snider et al., 2016), which causes not only haze and smog that lower visibility, but also respiratory and cardiovascular diseases that harm human health (Tie and Cao, 2009; Xing et al., 2016; Yang et al., 2019). In 2010 alone, an estimated 2.6 million premature deaths were associated with $PM_{2.5}$ pollution (Wang et al., 2017). Without proper controls, unbridled use of fertilizer to boost food production for the fast-growing population can further enhance global agricultural NH_3 emissions by ~12% in 2050 compared to year-2010 level, posing an even greater health risk via $PM_{2.5}$ formation (Bodirsky et al., 2014). Our public health system may have to spend 20–290 billion USD more each year to compensate for the NH_3-derived detrimental effects on air quality and health (Gu et al., 2012; Paulot and Jacob, 2014; Guthrie et al., 2018).

Excessive atmospheric NH_3 also threatens ecosystems. The highly soluble NH_3 gas and aerosol NH_4^+ (together known as NH_y) eventually return to the Earth's surface via dry and wet deposition, thus modifying the terrestrial nitrogen cycle. NH_y deposited on canopy foliage can be taken up and become readily available to promote photosynthesis (Wortman et al., 2012), but if highly concentrated it can also injure plant tissues and suppress biomass growth (Fangmeierfl et al., 1994; Krupa, 2003). Though NH_y deposition can enrich soil nutrients, it also brings several adverse effects, including soil acidification and forest biodiversity loss (Tian and Niu, 2015; Lu et al., 2008). Nitrifying bacteria often oxidize soil NH_4^+ in excess, and

https://doi.org/10.5194/bg-2021-63
Preprint. Discussion started: 16 March 2021

the resulting NO_3^-, which is prone to leaching, can lower soil nutrient content as well as contaminate groundwater, streams, rivers, and coastal waters, causing eutrophication (Lin et al., 2001; Beeckman et al., 2018). NH_y directly falling onto natural waters is potentially toxic to aquatic life even in low concentrations, and can deteriorate marine biodiversity (Zhang and Liu, 1994; Shou et al., 2018).

The severity of the aforementioned consequences of excessive reactive nitrogen in the environment has called for better management of these compounds, including better monitoring and mitigation of agricultural NH_3. Various technologies for measuring ambient NH_3 have been deployed since the last century (Erisman et al., 2001; Fowler et al., 2009). One such example is flux towers that combine laser detectors with an eddy-covariance method to provide on-site observations with finer time resolution (Sutton et al., 2008; Famulari et al., 2004; Ferrara et al., 2012; Zöll et al., 2016). Several national and international monitoring networks have also been established to obtain baseline ambient concentrations of NH_y, e.g., National Air Quality Monitoring Network in the Netherland (Buijsman et al., 1998), National Ammonia Monitoring Network (NAMN) in the UK (Sutton et al., 2005), National Atmospheric Deposition Program (NADP) in the US (Puchalski et al., 2011), European Monitoring and Evaluation Programme (EMEP) in Europe (Fagerli and Aas, 2008), and the Acid Deposition Monitoring Network in East Asia (EANET; https://www.eanet.asia/), to determine the rates of NH_4^+ deposition and NH_3 emission. Over remote areas, airborne (e.g., Nowak et al. (2010) and Leen et al. (2013)) and ship (e.g., Norman and Leck (2005) and Wentworth et al. (2016)) NH_y observations that combine near-field remote sensing and onboard in-situ measurement platforms have also been employed to fill the measurement gap. In the recent decade, the space-based Infrared Atmospheric Sounding Interferometer (IASI) has been deployed to gauge atmospheric NH_3 concentration within air columns (Clarisse et al., 2009). This new ensemble of satellite observations offers significant progress to address previous observational deficiencies and allows daily monitoring of global NH_3 distribution (Clarisse et al., 2010; Van Damme et al., 2014). Continued refinement in retrieval schemes and incorporation of machine-learning techniques have further improved the sensitivity and reliability of measured NH_3 concentrations (Van Damme et al., 2017). It enables the creation of near real-time high-resolution maps of atmospheric NH_3 and the possibility of pinpointing industrial and agricultural emission hotspots with diameters smaller than 50 km (Van Damme et al., 2018).

https://doi.org/10.5194/bg-2021-63
Preprint. Discussion started: 16 March 2021

Their works have provided valuable datasets not only for monitoring agricultural emissions but also for benchmarking and improving emission inventories and numerical models.

NH_3 emission inventories are generally compiled by surveyed activity data and empirical emission factors associated with primary sources including animal populations, synthetic nitrogen fertilizers, biomass burning, and natural sources. A 1º-by-1º inventory, which was among the first back then, estimated a global emission of 54 Tg-N yr^{-1} for 1990, of which 34 Tg-N yr^{-1} is agricultural, excluding field burning, and 2.4 Tg-N yr^{-1} from natural soil (Bouwman et al., 1997). Since then, much effort has been put into refining the estimation of anthropogenic emissions. Recent inventories adjusted the estimated agricultural emission in 2000–2008 to 33–37 Tg-N yr^{-1} (Sutton et al., 2013). One of the state-of-the-art inventories, the Emissions Database for Global Atmospheric Research (EDGAR) version 4.3.2, provides global anthropogenic emission estimates in 0.1º-by-0.1º resolution for the period 1970–2012 (Crippa et al., 2018). The accuracy of these inventories is not only affected by the integrity of the activity data surveyed, but also constrained by the suitability of emission factors. Simply adopting emission factors from other countries may result in biases because of regional differences in technologies, farming practices, climate, and soil conditions (Huang et al., 2012). This pitfall has motivated the development of other national and regional inventories in the US (e.g., US Environmental Protection Agency (2014)), China (e.g., Zhang et al. (2018)), and Europe (e.g., European Environment Agency (2013)). These emission inventories are useful tools for source apportionment and input data for forward models but as the NH_3 emissions are prescribed they do not respond to changes in, e.g., nitrogen deposition and meteorology, making them insufficient for models to represent the full dynamics of the NH_y cycle.

The global NH_y cycle has proven to be challenging to study because of the various feedback mechanisms within the Earth system. The reactive nature of NH_3 and the contribution of deposited NH_4^+ to the re-emission of NH_3 from natural and agricultural soils have created a convoluted relationship between emissions and deposition. NH_4^+ particles can be transported along with airflows and dispersed across a more extensive geographical range than the highly reactive gaseous NH_3. Such transport can introduce large heterogeneity in the spatial distribution of reactive nitrogen, rendering it not only a local but pan-regional problem (Willem Asman; Mark A. Sutton, 1998). Moreover, NH_3 volatilization is a temperature-dependent process while the presence of atmospheric NH_3 affects the composition of aerosols and their

https://doi.org/10.5194/bg-2021-63
Preprint. Discussion started: 16 March 2021

radiative forcing, thus in turn modifying the Earth's surface energy budget (Ansari and Pandis, 1998).

In this study, we hence aim to enable modeling of the land-atmosphere bidirectional exchange of NH_y, so that we can quantify the dynamically evolving NH_y cycle and feedback mechanisms associated with it under a changing environment. We employed the Community Earth System Model version 2 (CESM2), which has state-of-the-art model components representing the land, atmosphere, sea ice, and oceans. These sub-models can run independently or in various coupled configurations (Hurrell et al., 2013). Many studies have employed CESM for studying processes in both the atmospheric and terrestrial nitrogen cycles, e.g., NO_x and N_2O emission (Saikawa et al., 2013, 2014; Zhao et al., 2017), denitrification and nitrate leaching (Nevison et al., 2016), crop nitrogen uptake (Levis et al., 2018), and reactive nitrogen input to ecosystem associated with synthetic and manure fertilizers (Riddick et al., 2016). Yet, these studies did not consider the dynamic bidirectional transfer of NH_3 and NH_4^+ between the land and atmosphere. To add the dynamic cycle of NH_y back to CESM2, we adopted a process-based approach to parameterize NH_3 emission from cropland soils, which is different from the "voltage-resistance" models (Riddick et al., 2016; Vira et al., 2020). We also developed a prognostic parameterization for canopy capture of NH_3, instead of using a fixed generic value (e.g., one constant canopy reduction factor for all plants as used in many other studies (Riddick et al., 2016; Bouwman et al., 1997). Implementing these new schemes in the Community Land Model version (CLM5) (Lawrence et al., 2019), we could then estimate the emission associated with fertilizer use and perform fully coupled simulations with the Community Atmosphere Model version 4 with Chemistry (CAM4-Chem) (Lamarque et al., 2012) that allow two-way exchange of NH_y bridged by online emission and deposition to understand the subsequent effects on aerosol formation, climate, terrestrial ecosystems, and crop growth. We also compared our results with available emission inventories to evaluate model accuracy and uncertainty. This paper demonstrates a framework to unfold the complicated interactions between fertilizer use, NH_3 emission, aerosol formation, climate, terrestrial ecosystems, and crop production.

https://doi.org/10.5194/bg-2021-63
Preprint. Discussion started: 16 March 2021

2. Methods

2.1 Community Earth System Model

We introduced new functionalities into CESM2 to enable the simulation of a coupled land-atmosphere nitrogen cycle, and to further investigate the impacts of fertilizer-induced NH_3 emission on atmospheric composition, terrestrial biogeochemistry, and climate change. In particular, we implemented into CLM5 new parameterization schemes to quantify NH_3 volatilized from soil due to fertilizer application and captured by plant canopies. We further bridged CLM5 and CAM4-chem to enable two-way exchange of soil NH_3 emission and deposition of NH_4^+ to model a fully coupled, prognostic land-atmospheric NH_y cycle.

Our model development was based on CLM5 with active biogeochemical cycles and crop sub-model (CLM5-BGC-Crop or CLM5 in short), which represents terrestrial carbon and nitrogen cycling with prognostic vegetation and crop growth (Lawrence et al., 2019). The model uses a sub-grid hierarchy (from grid cells, land units, columns, to patches) to capture the biogeophysical and biogeochemical differences between various land types within a model grid cell. In particular, CLM5 handles natural soil and croplands differently: multiple natural vegetation patches are configured to occupy a single unmanaged soil column sharing a single pool of nutrients while each crop patch has a dedicated column. Such setting allows no resource competition between natural vegetation and crops, nor among crops (Drewniak et al., 2013). There are 16 types of natural vegetation (including bare ground) and eight active crops (temperate soybean, tropical soybean, temperate corn, tropical corn, spring wheat, cotton, rice, and sugarcane) in this model. Vegetation and crops are represented by plant functional types (PFTs), each having specific ecophysiological, phenological and biogeochemical parameters (Levis et al., 2018). Default PFT distribution of natural vegetation and crops are derived from satellite observations (e.g., MODIS) and agricultural census data (Lawrence and Chase, 2007; Portmann et al., 2010). The beginning of plant growth stages (seedling, leaf emerging, and grain filling), as well as crop sowing dates and planting durations, are controlled by cumulative warm-enough hours at the beginning of spring. Crops obtain nutrients from the soil mineral nitrogen pool, which is supplied by nitrogen deposition and fertilization. Fertilizer is applied to each patch for 20 consecutive days evenly when the crops enter the leaf emergence phase. Crops are harvested once they reach maturity or predefined maximum growing days (typically 150–165 days) (Lawrence et al., 2020).

https://doi.org/10.5194/bg-2021-63
Preprint. Discussion started: 16 March 2021

2.2 Soil ammonia emission and canopy capture

Figure 1 summarizes the primary pathways of the terrestrial nitrogen cycle in CLM5. The model tracks nitrogen content in soil, plant, and organic matter as an array of separate nitrogen pools, and biogeochemical processes as exchange fluxes of nitrogen between these pools. Soil mineral nitrogen, NH_4^+, and NO_3^- are competed for among plant uptake, microbial immobilization, nitrification, and denitrification, based on the relative demand from each process. Release of nitrous oxide (N_2O) and NO_x as byproducts of nitrification and denitrification and leaching of soil nitrate also deplete soil NH_4^+ and NO_3^-, which can be replenished by fertilization and deposition of atmospheric NH_y and NO_x. The deposition rates were prescribed in the default configuration and dynamically computed by CAM4-chem in our version. Other sources of soil mineral nitrogen include biological fixation by microbes or soybean and decomposition of plant litter and soil organic matter. Our proposed NH_3 emission scheme was derived from another standalone biogeochemical model, the DeNitrification-DeComposition (DNDC) model version 9.5 (Li et al., 2012), which has been used for studying agricultural NH_3 emission (Balasubramanian et al., 2015; Zhang and Niu, 2016; Balasubramanian et al., 2017).

https://doi.org/10.5194/bg-2021-63
Preprint. Discussion started: 16 March 2021

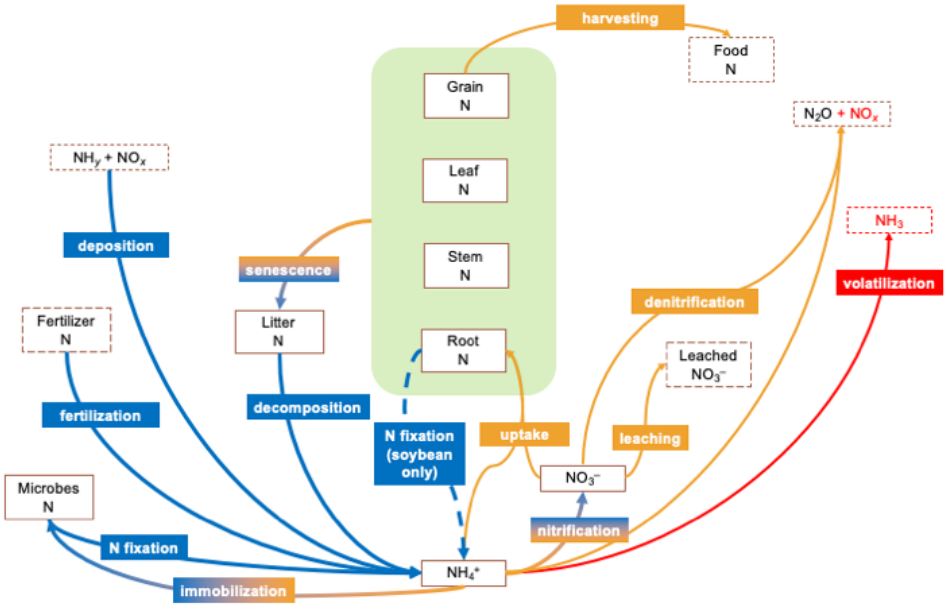

205 **Figure 1.** Major pathways modeled by CLM5 nitrogen (N) cycle. Blue arrows indicate N entering the soil N nitrogen pool while orange arrows are for leaving. The default model tracks only N pools in boxes enclosed by solid lines, but not those with dashed lines. N contents in crop tissues are modeled as pools inside the green regions. The red arrow indicates the missing pathway of NH_3 volatilization in the default model.

210 In our scheme, NH_3 volatilization is considered as a multistage process, and we estimated a potential soil NH_3 emission rate of each soil layer in each column or patch as:

$$\left.\frac{\mathrm{d}[\mathrm{NH_3\,(g)}]}{\mathrm{d}t}\right|_{\mathrm{soil}} = [\mathrm{NH_4^+\,(soil)}](1 - f_{\mathrm{ads}}) f_{\mathrm{dis}} f_{\mathrm{vol}} \left(\frac{1}{\Delta t}\right) \quad (1)$$

where $[NH_4^+\,(soil)]$ (g-N m^{-2}) is the amount of soil NH_4^+; Δt is model the time step size in CLM5 (default = 1800 s); f_{ads} accounts for the portion of NH_4^+ adsorbed onto the surface of soil matrix;
215 f_{dis} is the fraction of the non-adsorbed NH_4^+ that dissociated into aqueous NH_3, and; f_{vol} is the fraction of aqueous NH_3 volatilized as gaseous NH_3. The adsorbed fraction f_{ads} is given by:

$$f_{\mathrm{ads}} = 0.99(7.2733 f_{\mathrm{clay}}^3 - 11.22 f_{\mathrm{clay}}^2 + 5.7198 f_{\mathrm{clay}} + 0.0263) \quad (2)$$

where f_{clay} is soil clay fraction as prescribed by the CLM surface data (Bonan et al., 2002).

https://doi.org/10.5194/bg-2021-63
Preprint. Discussion started: 16 March 2021

The non-adsorbed NH_4^+ dissociates reversibly into aqueous NH_3 and hydrogen ion ($NH_{4(aq)}^+ \rightleftharpoons NH_{3(aq)} + H^+$), and hence, f_{dis} is determined by the following equations (Li et al., 2012):

$$f_{\mathrm{dis}} = \frac{K_{\mathrm{w}}}{K_{\mathrm{a}}[\mathrm{H}^+]} \quad (3)$$

$$K_{\mathrm{w}} = 10^{0.08946+0.03605T_{\mathrm{soil}}} \times 10^{-15} \quad (4)$$

$$K_{\mathrm{a}} = (1.416 + 0.01357T_{\mathrm{soil}}) \times 10^{-5} \quad (5)$$

$$[\mathrm{H}^+] = 10^{-\mathrm{pH}} \quad (6)$$

where K_a (in mol L^{-1}) and K_w (in mol L^{-2}) are dissociation constants for NH_4^+/NH_3 and hydrogen-/hydroxide-ion equilibria, respectively; T_{soil} (in °C) is soil temperature; $[H^+]$ (in mol) is the concentration of aqueous hydrogen ion in the soil calculated from soil pH. CLM5 is currently not capable of calculating soil pH implicitly so we performed our simulations using a constant pH of 6.5 for a more focused analysis. This pH value is consistent with the value used in the nitrification and denitrification schemes in CLM5 (Lawrence et al., 2019). We further evaluated the uncertainty induced by our choice of pH and presented the sensitivity test results in **Appendix**.

Lastly, we used this equation to calculate f_{vol}:

$$f_{\mathrm{vol}} = \left(\frac{1.5s}{1+s}\right)\left(\frac{T_{\mathrm{soil}}}{50+T_{\mathrm{soil}}}\right)\left(\frac{l_{\mathrm{max}}-l}{l_{\mathrm{max}}}\right) \quad (7)$$

where s (in m s^{-1}) is surface wind speed; T_{soil} (in °C) is soil temperature; l and l_{max} (both in m) are the depth of each particular soil layer and the maximum depth of a soil column, respectively. The actual soil NH_3 emission rate is then determined by the lower of the potential soil NH_3 emission rate or the available soil NH_4^+.

If vegetation is present above the soil, some of the emitted NH_3 can be retained by the plant canopy, which is known to be related to the adsorption of hydrophilic NH_3 onto the leaf surface and molecular diffusion via the leaf stomata (Van Hove et al., 1987). Some studies represented the amount of captured NH_3 using constant scaling factors (e.g., 0.6 for all vegetation in Riddick et al. (2016), 0.8, 0.5, and 0.2 for tropical rainforests, other forests, and

https://doi.org/10.5194/bg-2021-63
Preprint. Discussion started: 16 March 2021

all other vegetation types, respectively, in Bouwman et al. (1997)). Here, we calculated the flux of NH_3 captured by canopy following the equation used in DNDC that accounts for the change in in-canopy NH_3 concentration, deposition velocity of ammonia, leaf area index (LAI), and air moisture (Institute for the Study of Earth, Oceans, and Space, University of New Hampshire, 2017). To include the dynamic growth of crop canopy, we further adopted the canopy height adjustment factor employed by the Community Multiscale Air Quality (CMAQ) regional chemical transport model (Pleim et al., 2013). The change in in-canopy NH_3 concentration is thus:

$$\frac{\mathrm{d}[\mathrm{NH_3\,(g)}]}{\mathrm{d}t}_{\mathrm{canopy}} = \left(\frac{\mathrm{d}[\mathrm{NH_3\,(g)}]}{\mathrm{d}t}_{\mathrm{soil}}\right) f_{\mathrm{can}} \tag{8}$$

$$f_{\mathrm{can}} = \frac{L}{s_{10}} v_{\mathrm{c}} \varphi_{\mathrm{c}} b (h_{\mathrm{top}} - h_{\mathrm{bot}}) \tag{9}$$

where L is one-sided snow-free LAI, s_{10} is the wind-speed (in m s^{-1}) at 10-m height, v_c is the deposition velocity of NH_3 (0.05 m s^{-1} as in DNDC), φ_c is in-canopy relative humidity, b is a correction factor for the effect of canopy thickness (14 m^{-1} is used here as suggested by Pleim et al. (2013)), and h_{top} and h_{bot} are heights of canopy top and bottom (both in m), respectively. Except for v_c and b, all variables are calculated within CLM5 (see Lawrence et al. (2019) for detailed calculation methods). These two equations estimate the concentration of NH_3 exposed to plant canopy under a given soil emission rate at each time step: dividing soil NH_3 emission rate by s_{10} gives an approximate in-canopy NH_3 concentration, and multiplying the latter with v_c and L produces an estimated quantity of NH_3 retained by the canopy. The last three terms account for the influence of in-canopy moisture and canopy thickness on the effectiveness of canopy capturing. We subtracted this amount of captured NH_3 from the soil emission to obtain the quantity of NH_3 escaping to the above-canopy atmosphere, which was then used as input data to drive chemistry calculations in CAM4-chem. The captured NH_3 can re-enter the soil surface along with water throughfall or be metabolized by the plants if it diffuses into the leaf tissues (Hutchinson et al., 1972). Since the detailed mechanisms are still uncertain and beyond the focus of this study, we decided to assume that all captured NH_3 returns to the soil directly as NH_4^+ and will discuss how it will affect our analysis in **Conclusions**.

https://doi.org/10.5194/bg-2021-63
Preprint. Discussion started: 16 March 2021


Biogeosciences Discussions Open Access EGU

2.3 Emissions of other reactive nitrogen compounds

In addition to the NH_3 schemes, we also incorporated new equations to calculate NO_x released as by-products of nitrification and denitrification. The original CLM5 estimates the amount of N_2O leakage during nitrification by applying a constant scaling factor to the nitrification rate (Li et al., 2000) while that from denitrification is variable and evaluated by the DayCent approach (Del Grosso et al., 2000). Building on the work of previous studies (Parton et al., 2001, 2004; Zhao et al., 2017), we computed a ratio of NO_x to N_2O to account for the leaking of the former during nitrification and denitrification using the following equations:

$$NO_x{:}\,N_2O = 15.2 + \frac{35.5\tan^{-1}[0.68\pi(10D_r - 1.86)]}{\pi} \tag{10}$$

where D_r is the relative gas diffusivity in soil vs. in air and is calculated as a function of air-filled pore space (AFPS) of soil (Davidson and Trumbore, 1995):

$$D_r = 0.209\mathrm{AFPS}^{\frac{4}{3}} \tag{11}$$

$$\mathrm{AFPS} = 1 - \frac{\theta_V}{\theta_{V,sat}} \tag{12}$$

where θ_V and $\theta_{V,sat}$ are instantaneous and saturated volumetric soil water content (in $m^3\ m^{-3}$), respectively.

In addition, we added back the 20% of microbial mineralized nitrogen to the nitrification rate, which was missing in the previous versions of CLM, following the DayCent approach (Parton et al., 2001). We also applied a temperature factor to correct the overestimation of NO_x emission at high latitudes as suggested in some previous studies (Xu and Prentice, 2008; Zhao et al., 2017):

$$f_T = \min\left(1, e^{308.56\left(\frac{1}{68.02} - \frac{1}{T_{soil}+46.02}\right)}\right) \tag{13}$$

where T_{soil} is soil temperature measured in Kelvin (K) here.

https://doi.org/10.5194/bg-2021-63
Preprint. Discussion started: 16 March 2021

2.4 Simulations of the land-atmosphere NH_y cycle

For the atmospheric component, we employed CAM4-chem, with chemistry based on the tropospheric chemistry mechanism of MOZART-4 (Emmons et al., 2010). CAM4-chem employs a bulk aerosol approach and predicts the formation of $PM_{2.5}$ components including SO_4^{2-}, NO_3^-, and NH_4^+, where the injection rates of precursors – sulfur dioxide (SO_2), NO_x, and NH_3 – are prescribed by Coupled Model Intercomparison Project phase 6 (CMIP6) emission inventory for anthropogenic activities as well as some natural sources in the default configuration (Hoesly et al., 2018). Biogenic emissions are updated online from CLM5 using the Model of Emissions of Gases and Aerosols from Nature (MEGAN) version 2.1 (Guenther et al., 2012). In our coupled simulations, we omitted the portion of NH_3 emission associated with synthetic fertilizer from the inventory input for CAM4-chem and replaced it with our online simulated emission rates from CLM5. Atmospheric NH_3 and NH_4^+ formed sequentially return to CLM5 through deposition.

Dry deposition in CAM4-chem is handled using the resistance approach (Wesely, 1989; Emmons et al., 2010). For NH_3 vapor, the model calculates the aerodynamic and the boundary-layer resistance based on the online atmospheric dynamics, while the surface resistance over land is determined according to the online CLM5 surface variables, e.g., canopy height and LAI, as well as species-specific reactivity factor for oxidation and effective Henry's Law coefficients. For particle-phase NH_4^+, the aerodynamic resistance is the same as that of NH_3, but the boundary-layer and surface resistances are replaced by a single resistance term that depends on the surface friction velocity. The deposition velocities of NH_3 and NH_4^+ are the reciprocal of the sum of their corresponding resistance terms, and their deposition rates are the product of their deposition velocities and concentrations. Wet deposition in CAM4-chem follows the Neu and Prather (2012) scheme, which assumes a first-order loss of chemicals due to in-cloud and below-cloud scavenging processes. The wet deposition rates of NH_3 and NH_4^+ are the products of their concentration, their loss frequencies (based on their Henry's Law coefficients), and the fraction of the grid box subject to scavenging (e.g., cloudy or raining). These NH_y deposition fluxes then become the input to CLM5 as soil NH_4^+ (Lawrence et al., 2020).

Recent studies on NH_3 emission using CESM2 (e.g., Riddick et al. (2016) and Vira et al. (2020)) focused only on the one-way land-to-atmosphere flux of NH_3 while neglecting the

https://doi.org/10.5194/bg-2021-63
Preprint. Discussion started: 16 March 2021

enhancing effect of nitrogen deposition on NH_3 emission. By coupling CLM5 and CAM4-chem, we allowed, for the first time, the model land-atmosphere NH_y cycle to evolve in response to any changes in the bidirectional exchange of NH_3 and NH_4^+ via online emission and deposition. It also makes our method more suitable than a one-way model for studying the feedback effects of future changes in climate and agricultural activities on the biogeochemical cycles.

Table 1 provides configuration details of our experiments. All simulations were run for 10 years using year-2000 initial conditions with the corresponding land cover data. The first five years of outputs were used as model spin-up, and thus, our analysis in the next section focused on the last five years of simulated results. The spatial resolution of our simulations was 1.9º by 2.5º horizontally with 32 layers of atmospheric layers from the surface to up to ~40 km, and 25 soil layers down to ~50 m below ground. Our analysis focused on the changes in fluxes of soil biogeochemical processes, the evolution of atmospheric NH_3, NH_4^+, and other SNA aerosols, and the influence of the bidirectional NH_y exchange on crop production. Fertilizer input was prescribed by crop type and country at the 2000-level based on Land-Use Harmonization (LUH2) fertilization rates (Hurtt et al., 2011). All fertilizers added were assumed synthetic and no manure was included.

Table 1. Details of simulation designs.

Name	Fertilizer-induced NH_3 Emission	N-deposition	Aerosol-radiation Interaction
CAM4_CLM5	This study	Dynamic	Enabled
CAM4_CLM5_NDEP	This study	Dynamic	Disabled
CAM4_CLM5_CLIM	This study	From [CAM4_CLM5] assuming 2000-level fertilization	Enabled
CAM4_CMIP6	CMIP6 inventory	Dynamic	Enabled

2.5 Datasets for model validation

We also compared our simulation results with various available observations and emission inventories. CLM5-modeled NH_3 emission was compared with multiple emission inventories including CMIP6, EDGAR, and the Magnitude And Seasonality of Agricultural Emissions for

https://doi.org/10.5194/bg-2021-63
Preprint. Discussion started: 16 March 2021

NH_3 (MASAGE). CAM4-chem-simulated atmospheric NH_3 using CLM5 NH_3 and CMIP6 were compared against the satellite-derived IASI-NH_3 concentration field (gridded and reported in Van Damme et al. (2018). Details of these datasets are tabulated in **Table 2**. The datasets were regridded to match our model resolution of 1.9º by 2.5º using bilinear interpolation.

Table 2. Details of observations and emission inventories used in this study for model comparison and validation.

Name	Coverage	Resolution	Period of data	Data type: sources extracted for model comparison
MASAGE (Paulot et al., 2014)	Global	0.5º-by-0.5º Monthly mean	2006	Emission inventory: NH_3 emission from agricultural soil associated with synthetic fertilizers for crops
EDGAR (Crippa et al., 2018)	Global	0.1º-by-0.1º Monthly mean	2010	Emission inventory: NH_3 emission from agricultural soil with fertilizer and manure application
CMIP6 (Hoesly et al., 2018)	Global	0.01º-by-0.01º Monthly mean	2006–2015	Emission inventory: NH_3 emission from agricultural soil with fertilizer and manure application
IASI (Van Damme et al., 2018)	Global	0.01º-by-0.01º Annual mean	2008–2016	Satellite-based measurement: Column NH_3 density

3. Results

3.1 Fertilizer-induced NH_3 emission

We first evaluated the fertilizer-induced NH_3 emission simulated by the fully coupled land-atmosphere simulation, [CAM4_CLM5]. **Figure 2** shows the annual-total global NH_3 emission at above-canopy level from different land types averaged over the last five years of simulation. We also compared our NH_3 emission with inventory estimates reported by CMIP6 (Hoesly et al., 2018), EDGAR v4.3.2 (Crippa et al., 2018), and MASAGE (Paulot et al., 2014). We extracted the monthly fertilizer-induced NH_3 emission estimates from MASAGE, and assumed that one-third of the total agricultural NH_3 emission reported by CMIP6 and EDGAR are fertilizer-associated, which is consistent with the apportionment reported in previous studies and environmental reports (Paulot et al., 2014; Riddick et al., 2016; National Oceanic and Atmospheric Administration, 2000; European Environment Agency, 2010; Gu et al., 2012; Paulot et al., 2015; Zheng et al., 2017).

https://doi.org/10.5194/bg-2021-63
Preprint. Discussion started: 16 March 2021

A grid cell-by-grid cell model-inventory spatial comparison of the annual-total NH_3 emission rates was conducted by computing Pearson's correlation coefficients (R) and slopes (β) of linear regression using the reduced major axis method as well as normalized mean biases (NMB; $\Sigma(M_i - O_i)/\Sigma(O_i)$, where M_i and O_i are simulated and inventory NH_3 emission in each grid cell) and mean fractional biases (MFB; $2\Sigma[(M_i - O_i)/(M_i + O_i)]/N$, where N is the number of grid cell). A summary of these statistics is shown in **Fig. 2(a)**. We also computed the R values between the monthly emission rates computed by CLM5 (as in the fully coupled case, [CAM4_CLM5]) and each inventory for each grid cell (see **Fig. 2(d)**, **(f)**, and **(h)**). We highlighted with overlaying black dots the grid cells with high coefficients of determination, which are statistically significant (i.e., $R^2 > 0.5$ and $p < 0.05$), indicating where our simulation can reproduce more than half of the variability of the inventory estimates.

Globally, CLM5 estimates that the annual-total fertilizer-induced NH_3 emission reaches 11 Tg-N yr^{-1}, which is close to the 12 Tg-N yr^{-1} and 11 Tg-N yr^{-1} reported by the two similar studies, Riddick et al. (2016) and Vira et al. (2020), respectively. Our estimate is slightly higher than all three inventories, which are 10 Tg-N yr^{-1} for CMIP6 and EDGAR, and 9.1 Tg-N yr^{-1} for MASAGE. The global R values are positive and lie within 0.5–0.6 across all inventories, indicating a fairly good correlation between CLM5 and all three inventories, especially CMIP6 and MASAGE. Systematic model high-biases are implied by the greater-than-unity β values. Such high-biases are within acceptable levels as the NMB values are smaller than 200% and the magnitudes of MFB values are within 50% (Boylan and Russell, 2006).

Top food-producing countries are responsible for a major portion of the fertilizer-induced NH_3 emission: 26% of CLM5 global total was from India, 17% from the US 17%, and 9.7% from China. Emission hotspots are found close to their cropping regions in the model and the inventories, but their spatial gradients are different. In India, CLM5 shows more concentrated emission sources over the northern regions, resulting in higher local emission rates than the inventories. This distribution pattern resembles the India's north-higher south-lower fertilization gradient adopted by the model. In contrast, CMIP6 estimates a more evenly distributed emission spatial pattern over India, and higher emission rates over the southern regions. EDGAR and MASAGE show a spatial gradient of NH_3 emission decreasing from north to south. Such gradients may explain their low R and high β values against our revised

https://doi.org/10.5194/bg-2021-63
Preprint. Discussion started: 16 March 2021

CLM5. Despite the spatial mismatch, model estimation over India still falls in the acceptable range in terms of the regional NMB and MFB.

CLM5 estimates more intense emission hotspots in the US, which are located near the "Corn Belt" of the central US and southern California. US emission rates by CLM5 are much higher than the other three inventories, as seen in the difference maps in **Fig. 2**, as indicated by the large β (>2.5), and large regional NMB. Differences in the spatial distribution of NH_3 emission are also observed over China. CLM5 estimates that more NH_3 is emitted from central and northeastern China, while the emission hotspots in CMIP6 and EDGAR are found in northeastern China and those of MASAGE are located in eastern China. Such deviation may be attributable to different fertilizer usage schedules used by CLM5 and other inventories. For example, MASAGE considers multiple-type fertilizers including ammonium bicarbonate, which is more prone to NH_3 loss than urea, and assumes a three-stage fertilization at sowing, growth, and harvesting (Paulot et al., 2014). EDGAR also reported a high uncertainty (~97%) of present-day NH_3 emissions in China due to incomplete information about the agricultural sector (Crippa et al., 2018).

https://doi.org/10.5194/bg-2021-63
Preprint. Discussion started: 16 March 2021

Biogeosciences
Discussions
Open Access
EGU

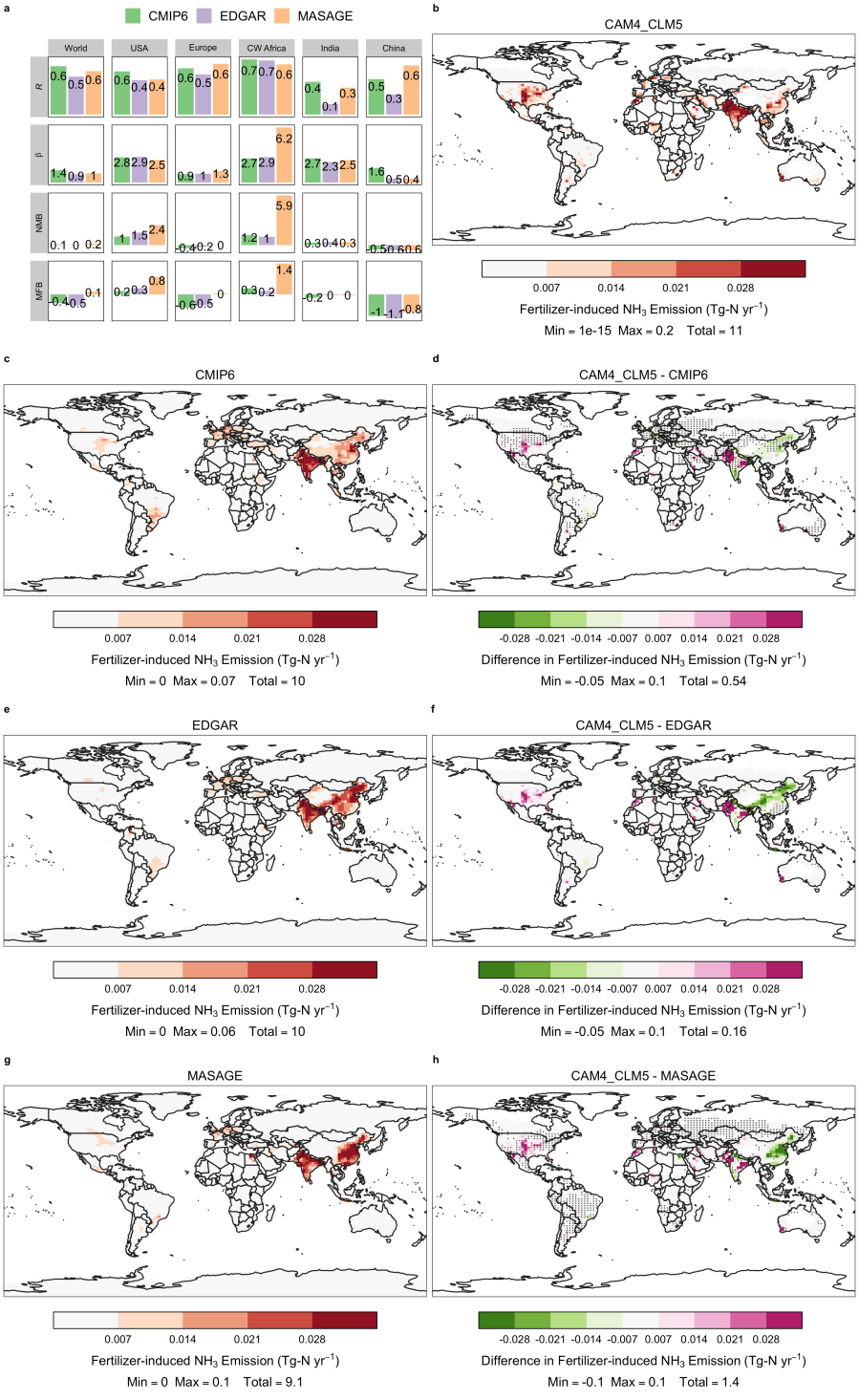

https://doi.org/10.5194/bg-2021-63
Preprint. Discussion started: 16 March 2021

415 **Figure 2.** Fertilizer-induced NH_3 emission estimated by CLM5 and other emission inventories. Correlation analysis between CLM5-simulated annual-total emission and other inventories with regional breakdowns is summarized in panel **(a)**. Spatial distribution of annual-total fertilizer-induced NH_3 emission simulated by [CAM4_CLM5], and estimated by CMIP6, EDGAR, and MASAGE are illustrated in panels **(b)**, **(c)**, **(e)**, and **(g)**, respectively. Panels **(d)**, **(f)**, and **(h)** show the spatial distribution of differences in annual-total NH_3 between
420 CLM5 and CMIP6, EDGAR, and MASAGE, correspondingly. Overlaying black dots in the difference maps indicate grid-cells with a high statistically significant spatiotemporal correlation (i.e., $R^2 > 50\%$, $p < 0.05$) between CLM5 and the corresponding inventories. Color scales are saturated at respective values, and ranges of values are shown in the legend titles.

425 **Figure 3** shows the seasonality of NH_3 emission associated with artificial fertilizer in the Northern and Southern Hemisphere. CLM5 assumes each crop receives a specific amount of fertilizer (as soil NH_4^+) applied evenly for 20 consecutive days since leaf emergence. This soil NH_4^+ input speeds up plant uptake, microbial immobilization, nitrification, as well as NH_3 volatilization, explaining the Northern Hemisphere peaking in emission in April and May and
430 Southern Hemisphere peaking in October, overlapping with the regional cropping seasons. All inventories show springtime peaks in each hemisphere, but the peak of EDGAR always leads the others by a month. CMIP6 has multiple peaks (two in the Northern Hemisphere and three in the Southern Hemisphere). These deviations exist mainly because of the differences in planting schedule and duration of fertilization used by the inventories. The higher CLM5 peaks
435 are consistent with the systematic overestimation discussed above. NH_3 emission returns to "background" levels when it is not in the planting seasons. EDGAR and CMIP6 have higher background levels because the original estimates accounted for not only synthetic fertilizer but also manure application (for both) and management (for CMIP6 only), which are not necessarily in phase with the cropping seasons (Huijsmans et al., 2018).

440 We concluded our model-inventory comparison by computing the correlation of monthly NH_3 emission rates in each model grid cell (see **Fig. 2(d)**, **(f)**, and **(h)**). CLM5 can capture a large portion of emission hotspots of CMIP6 over the US, Europe, India, China, and South America. With MASAGE, our estimate shows good agreement over mid-range emission regions, in North America, South America, Europe, and Southern Africa. CLM5 differs the
445 most from EDGAR among the three inventories. The resemblance with CMIP6 and MASAGE indicates that our NH_3 scheme has allowed CLM5 to produce reasonable NH_3 emission inputs

https://doi.org/10.5194/bg-2021-63
Preprint. Discussion started: 16 March 2021

for CAM4-chem simulations over most high to medium emission hotspots. It is also noteworthy that the magnitude and spatial distribution of NH_3 emission among inventories are also not consistent. Since environmental conditions control the rate of biological and chemical processes that release NH_3, processes such as urea hydrolysis and NH_4^+/NH_3 equilibrium can induce further inventory uncertainties (Hoesly et al., 2018). Inter-inventory uncertainties are also attributable to the choice of global and/or regional emission factors, which is crucial to reflect different agricultural procedures across the world, such as fertilization methods and fertilizer types, but not always well represented in global inventories (Paulot and Jacob, 2014; Riddick et al., 2016; Zhang et al., 2018).

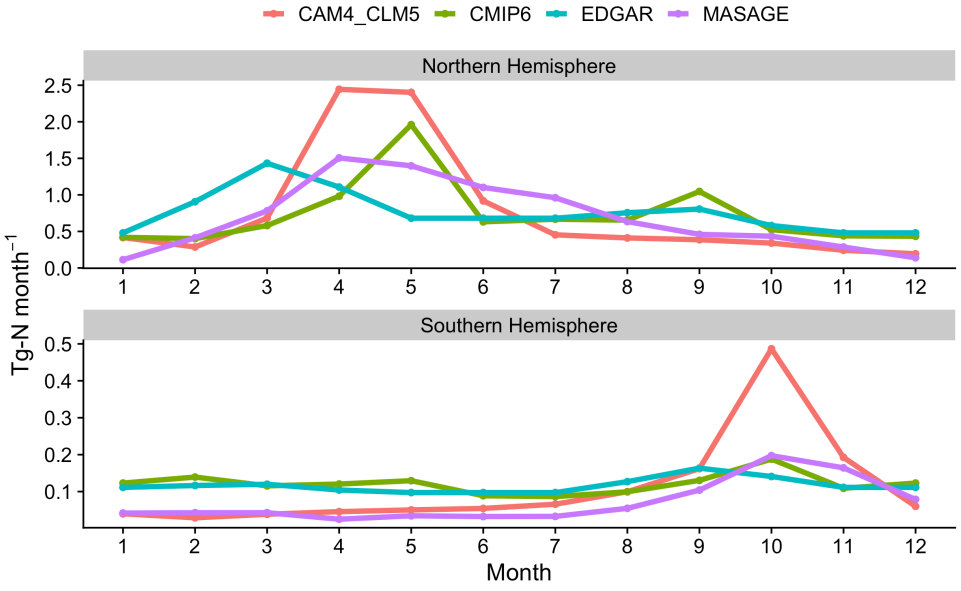

Figure 3. Monthly NH_3 emission associated with synthetic fertilizer use in the Northern and South Hemisphere estimated by CLM5, CMIP6, EDGAR, and MASAGE.

3.2 Atmospheric NH_3 concentration

Previous studies have evaluated the reactive nitrogen processes in CESM against satellite and ground observations, e.g., depositional fluxes of NH_3 and NH_4^+ (Lamarque et al., 2013), and

https://doi.org/10.5194/bg-2021-63
Preprint. Discussion started: 16 March 2021

ground concentration of gaseous NH_3 (Hu et al., 2015). Here, we estimated the CAM4-chem simulated annual-mean atmospheric NH_3 using two different inputs of fertilizer-induced emissions simulated by our revised CLM5, and prescribed from CMIP6, which are aliased as [CAM4_CLM5] and [CAM4_CMIP6], respectively. **Figure 4** shows these results, aggregated to column total NH_3, alongside the 8-year annual-average IASI satellite retrievals.

Both simulations can capture the high concentration zones observed by IASI over the US, South America, and Western Europe, with global and regional R values > 0.8, indicating a good correlation between the modeled results and observations. However, both [CAM4_CLM5] and [CAM4_CMIP6] NH_3 are generally lower than IASI. Over the US and India, [CAM4_CLM5] estimates lower NH_3 concentration than that from IASI (regional β = 0.5–0.8), where CLM5 estimates high emission rates. Even more significant underestimation is seen in [CAM4_CMIP6] (regional β = 0.2–0.5), except in China, where lower emission rates are predicted by [CAM4_CLM5] (**Fig. 2(d)**). The magnitudes of NMB and MFB of [CAM4_CMIP6] are also more negative than [CAM4_CLM5], reflecting that using CLM5 as NH_3 emission input reduces the model NH_3 underestimation of CAM4-chem with the default CMIP6 inventory.

Mild differences are seen in North America and northeastern China, which are both intense agricultural regions; the discrepancies are likely attributable to the mismatch in crop growth map between CLM5 and the real world. Larger differences are shown over India and Western Europe, indicating the low-biases in the model of emission from tropical biomass burning regions (Whitburn et al., 2017; Van Damme et al., 2018).

We further compared the NH_3 burden of a run with online NH_3 emission and prescribed N deposition, i.e., [CAM4_CLM5_CLIM], against IASI to examine whether enabling the online bidirectional exchange can improve the estimation of NH_3 in CLM5. Turning on nitrogen deposition, the [CAM4_CLM5]-estimated global-total NH_3 emission is 0.6% higher than [CAM4_CLM5_CLIM]. Regional changes in NH_3 emission are not uniform (**Fig. S1**). The most prominent changes are found in Asia (+0.09 Tg-N yr^{-1} or +1.6%), and South America (–0.09 Tg-N yr^{-1} or –8.0%). When compared with IASI, [CAM4_CLM5] has closer-to-one β and closer-to-zero NMB and MFB than [CAM4_CLM5_CLIM], indicating that the fully coupled N-cycle could reduce model low-bias (**Fig. S2**).

https://doi.org/10.5194/bg-2021-63
Preprint. Discussion started: 16 March 2021

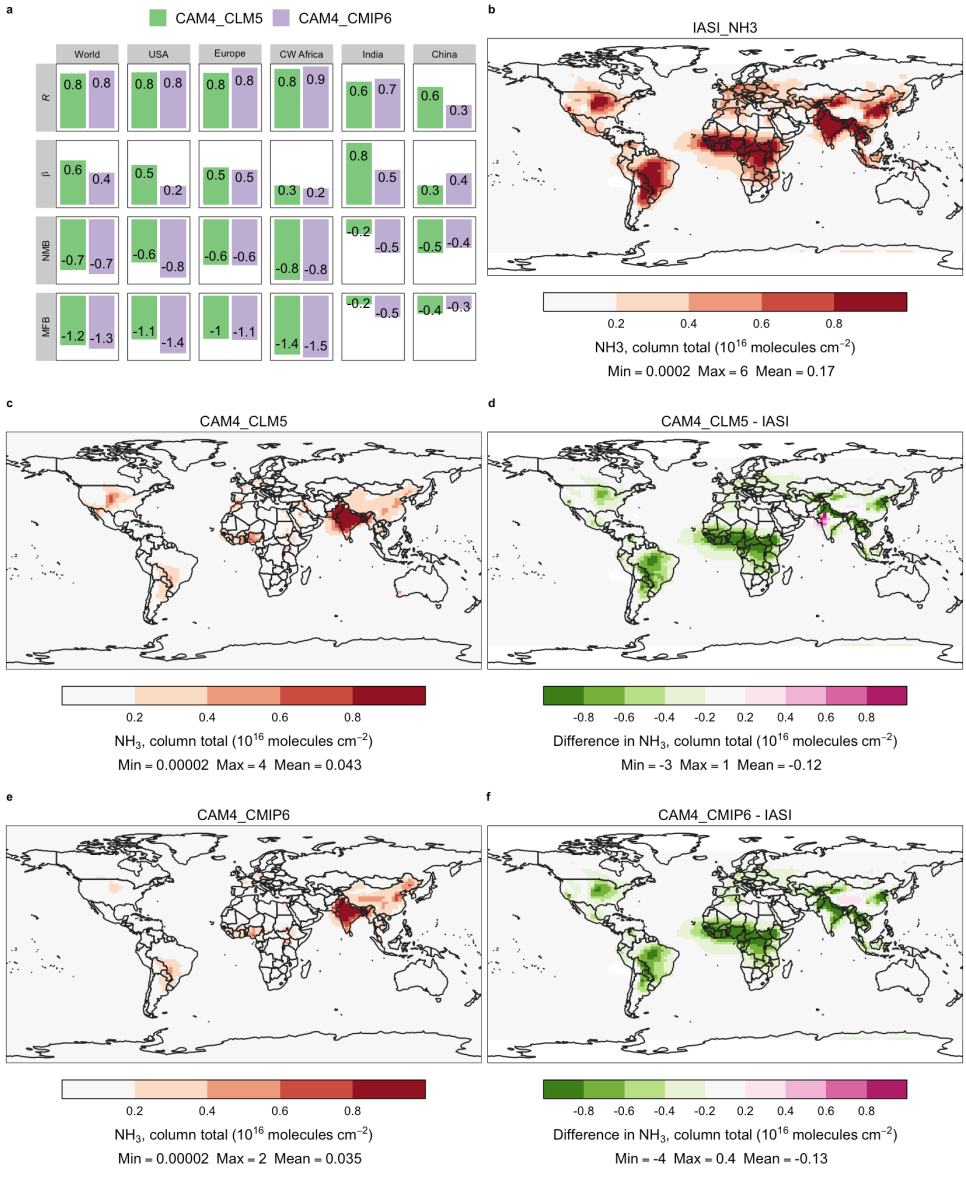

Figure 4. Annual-mean atmospheric NH_3 estimated by CAM4-chem with online CLM5 simulation and CMIP6 emission inventory as inputs of fertilizer-induced NH_3 emission, which are aliased as [CAM4_CLM5] and [CAM4_CMIP6], respectively. Panel **(a)** summarizes the correlation analysis between the two simulations and the IASI satellite retrievals. Panels **(b)**, **(c)**, and **(e)** show the column NH_3 concentration of IASI and the two cases correspondingly. Panels **(d)**, and **(f)** show concentration differences between each case and the IASI observations. Color scales are saturated at respective values, and ranges of values are shown in the legend titles.

https://doi.org/10.5194/bg-2021-63
Preprint. Discussion started: 16 March 2021

3.3 When fertilizer application is increased by 30% – a case study to reveal the importance of nitrogen deposition and aerosol-climate effect on NH_3 emission and grain production in a future scenario

Fertilizer use is predicted to increase by >30% of 2000-level to boost grain production to meet the fast-growing food demand by 2050 (FAO, 2007). Such injection of soil nitrogen will not only enhance soil NH_3 emission, but also alter atmospheric NH_4^+ formation and its subsequent climate effects and deposition, which will induce secondary impacts on crop growth and NH_3 re-emission. Here, we used the modified CLM5 and CAM4-chem to attribute such secondary impacts to nitrogen deposition and aerosol-climate effect. We performed this case study by scaling up the amounts of fertilizer application by 30% globally as input to the simulations detailed in **Table 1**.

[CAM4_CLM5] encapsulates the full functionality of our implementation, i.e., that CAM4-chem receives the online CLM5 NH_3 emission rates as input to predict atmospheric NH_3 concentration, the subsequent formation of ammonium salts, and the corresponding instantaneous aerosol radiative effect on climate, whilst CLM5 obtains the online CAM4-chem dry and wet deposition rates of NH_y and NO_x to calculate the addition of soil NH_4^+ via deposition. Such deposition will eventually enrich soil fertility and fuel the re-emission of soil NH_3 while the aforementioned aerosol radiative effect can cool the Earth's surface and suppress NH_3 volatilization. [CAM4_CLM5_CLIM] was prescribed with constant nitrogen deposition fluxes so that we could quantify the instantaneous aerosol radiative effects. Similarly, [CAM4_CLM5_NDEP] was configured such that addition/reduction of atmospheric NH_3 would not induce changes in aerosol-climate interactions, so that we could isolate the impact of NH_y deposition on NH_3 emission and crop growth.

Figure 5 shows the changes in annual-total fertilizer-induced NH_3 emission estimated by these simulations when the global fertilizer use rises to 130% of the 2000 level. The fully coupled case, [CAM4_CLM5], estimates that the global emission will rise by 2.4 Tg-N yr^{-1} or 23% more of fertilizer-associated NH_3 emission than the baseline case, i.e., [CAM4_CLM5] with 2000-level fertilization (see **Fig. 2(b)**). The nonlinear increase in emission relative to the fertilizer increment is expected because of the handling of fertilizer in CLM5 – fertilizer is

https://doi.org/10.5194/bg-2021-63
Preprint. Discussion started: 16 March 2021

added as NH_4^+ to soil evenly over 20 days when crop leaves begin to emerge, during which the NH_4^+ will be competed for among nitrification, plant uptake, microbial immobilization, as well as volatilization (as illustrated in **Fig. 1**). Our model modifications enabled CLM5 to simulate the dynamic competing processes depending on microbial activities, plant growth, and soil microclimate, as well as depositional soil nitrogen input and overlying climatic changes.

With constant nitrogen deposition fluxes, [CAM4_CLM5_CLIM] shows that NH_3 emission could increase by 2.5 Tg-N yr^{-1} from the baseline case under the future scenario. Comparing with [CAM4_CLM5], we find that, if aerosol-climate interactions are the only factor in play, NH_3 is reduced in the north-central US but increases in the south-central US (see **Fig. S3**). Such regional gradient is attributable to the north-south difference in plant uptake – higher plant uptake leaves less NH_3 to undergo volatilization.

When the emitted NH_3 and the subsequently formed aerosols are not allowed to affect climate radiatively, changes in [CAM4_CLM5_NDEP] are solely driven by the changes in nitrogen deposition, and such an effect enhances global NH_3 by 2.7 Tg-N yr^{-1}. These amplifying effects are most prominent in India, which CLM5 determines as an emission hotspot, driving a net increase by 1.6 Tg-N yr^{-1} in Asia relative to the baseline. Overall, we observe that nitrogen deposition leads to higher magnitudes of positive changes in NH_3 emissions than aerosol climate effects in all regions, except in the US. The smaller increment in the US is likely due to the lower surface temperature over the high-emission Corn Belt region (**Fig. S5**) that suppresses NH_3 volatilization.

Though the 30% addition of fertilizer use increases NH_3 emission in all cases, the changes in [CAM_CLM5] are not the simple mean of the two other cases, implying that the combined effect of nitrogen deposition and aerosol-climate interactions is nonlinear. For instance, the lower surface temperature over the US Corn Belt is associated with higher latent heat flux (**Fig. S7**), which is likely a consequence of better vegetation growth driven by increased NH_y deposition following higher NH_3 emissions. This fertilizing feedback effect via N deposition is not seen in [CAM4_CLM5_CLIM], which receives constant, prescribed N deposition fluxes. Such a nonlinear feedback effect highlights the importance of a land-atmosphere coupled model, as in CESM2, when considering the environmental and climate impacts of agricultural NH_3.

https://doi.org/10.5194/bg-2021-63
Preprint. Discussion started: 16 March 2021

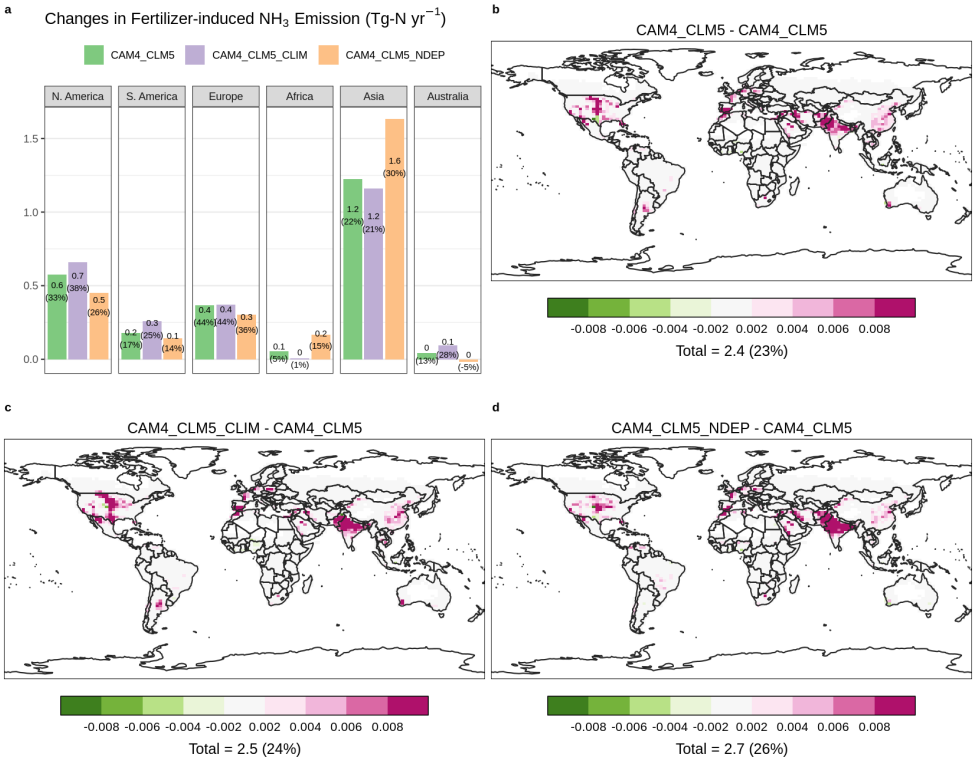

Figure 5. Changes in annual-total fertilizer-induced NH_3 emission after a 30% fertilization increase relative to [CAM4_CLM5] with 2000-level fertilization.

This nonlinearity is also exhibited in simulated grain production. CLM5 assumes a harvest efficiency of 85% (Lawrence et al., 2020). [CAM4_CLM5] estimates that, with nitrogen deposition and aerosol climate effect, 200 Tg yr^{-1} more grain is produced than the control (see **Fig. 6**). Such enhancement is found dominantly over the food-producing regions over the US Corn Belt and Western Europe, resulting in net regional increases by 54 Tg yr^{-1} and 108 Tg yr^{-1} in North America and Europe, respectively. It is noteworthy that the combined effect has a divergent impact and leads to production loss in South America, Africa, and Australia. Looking into the two other cases, [CAM_CLM_NDEP] shows that nitrogen deposition contributes to a large grain increase in Asia, North America, and Europe, which is a direct benefit of the extra input of soil NH_4^+ for crop growth improvement. Changes in [CAM_CLM5_CLIM] indicate that the aerosol climate effect offsets the intensified fertilization in virtually all continents, except in South America and Australia, which may be

https://doi.org/10.5194/bg-2021-63
Preprint. Discussion started: 16 March 2021

attributable to the prolonged growing period and shortened grain filling stage. For example, as seen in **Fig. S6**, surface temperature in North America is lower in [CAM4_CLM5_NDEP] than [CAM4_CLM5], and such cooler surface is associated with higher yield increases over the region as shown in **Fig. S5**. These results show that the combined impacts of the two processes not only vary nonlinearly but are also spatially uneven.

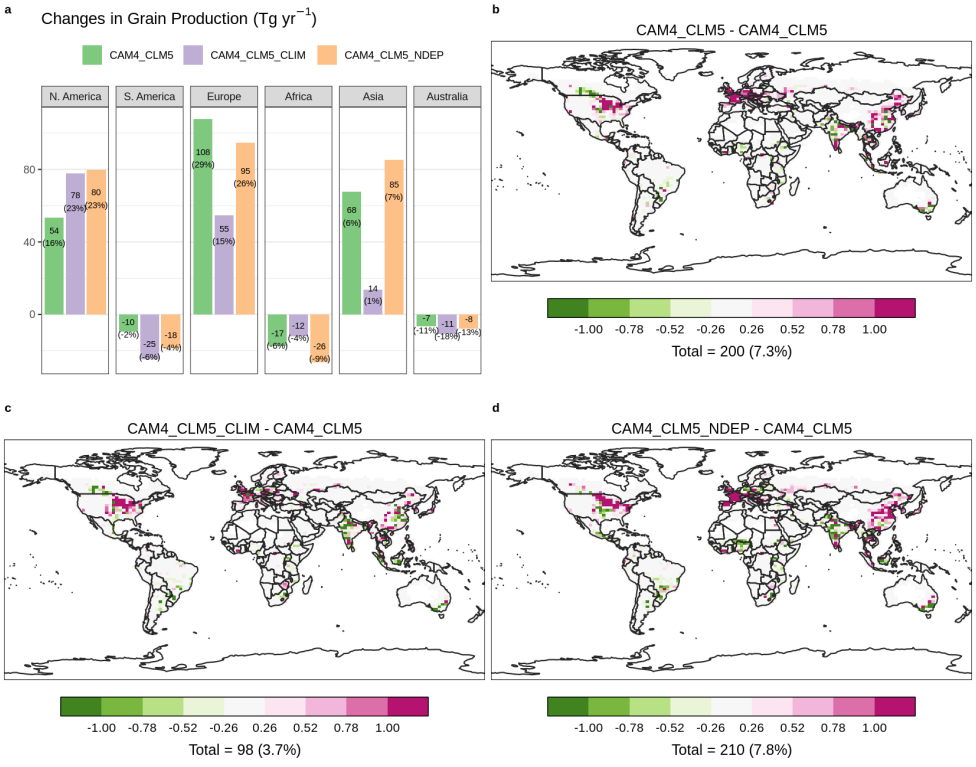

Figure 6. Same plots as **Fig. 5** but for annual-total grain production.

4. Conclusions

In this study, we implemented into the land and biogeochemical model, CLM5, new mechanistic schemes to better represent fertilizer-induced NH_3 emission from agricultural soil. Our modifications allowed CLM5 and CAM4-chem to dynamically exchange fluxes associated with reactive nitrogen deposition and NH_3 emission. These new features enabled CESM2 to

https://doi.org/10.5194/bg-2021-63
Preprint. Discussion started: 16 March 2021

perform, for the first time, a more reliable estimation of soil NH_3 emission and atmospheric NH_3 concentration under dynamic climate and environmental conditions. We verified that a fully coupled simulation case, [CAM4_CLM5], produced an estimation of NH_3 emission that agrees fairly well spatially and temporally with the emission inventories, MASAGE (Paulot et al., 2014) and CMIP6 (Hoesly et al., 2018), especially over high-emission regions (see **Fig. 2**). When compared to the IASI satellite observations (Van Damme et al., 2018), online NH_3 emission input in CLM5 reduces the low-biases exhibited in CAM4-chem estimation of atmospheric NH_3 using the CMIP6 NH_3 emission inventory.

Our modifications also enabled us to understand how NH_3 emission influences aerosol formation and aerosol radiative effect, and their secondary impacts on the re-emission of NH_3 and grain production. Our fully coupled simulation, [CAM4_CLM5], re-creates the spatial distribution of the emission hotspots observed by satellite over intensive agricultural regions including China, India, Europe, and the US (see **Fig. 4**). We estimated that the effect of nitrogen deposition on NH_3 emission is +2.7 Tg-N yr^{-1} globally, and is adjusted to +2.4 Tg-N yr^{-1} when the aerosol-climate effect is accounted for as well, compared with the baseline case (see **Fig. 5**).

This study demonstrates a modeling approach to estimate the climatic and environmental sensitivity of NH_3 emission, with a focus on sources associated with synthetic fertilizer only. Other primary sources of atmospheric NH_3 include manure management and application (47%), ocean (16%), and biomass burning (11%). (Bouwman et al., 1997; Sutton et al., 2013; Paulot et al., 2014, 2015). Unlike soil emission whereby the volatilization of NH_3 depends on a series of biogeochemical processes, emissions associated with manure management from confined facilities, e.g., animal factories, are easier to track. To quantify such emissions, one can collect activity data and emission factors from factory managers, and install monitoring instruments at facility outlets (Bouwman et al., 1997; Paulot et al., 2014). Manure usage for fertilizing croplands can be collected by surveying practices adopted by farmers. Its associated NH_3 emission can be estimated using source-specific emission factors and weather data, especially dominant factors such as air temperature, wind speed, and humidity. Fire emission directly injects the reactive nitrogen into the atmosphere, and satellite measurement is capable of capturing such short-term ammonia blooms (Van Damme et al., 2017). We did not include manure application in our study due to the high uncertainty and data

https://doi.org/10.5194/bg-2021-63
Preprint. Discussion started: 16 March 2021

insufficiency for validation. It is noteworthy that manure fertilizer is attributable up to ~25% of total NH_3 emission (Riddick et al., 2016) and hence shall warrant further research efforts in terms of its downstream impact on ecosystems via nitrogen deposition and aerosol radiative effect.

We also incorporated a prognostic parameterization for canopy capture of the emitted NH_3, which is an improvement when compared to previous studies that assigned blanket reduction factors to all vegetated land types (Bouwman et al., 1997; Riddick et al., 2016; Vira et al., 2020). Despite such addition, our model still shows systematic high-biases, implying room for improvement, including further calibration of the canopy capture effects against field measurements. Another source of uncertainties stems from the model's initial soil NH_4^+ content, which determines the potential emission rate of NH_3. The overestimation by CLM5 in this study may point to the more-fertile-than-reality soil conditions in the model, highlighting the need for a more realistic soil nitrogen map compiled by field surveys. We also note that such field surveys would also be useful to infer a soil pH map that constraints the uncertainty in simulations using a constant pH, like those reported in this study.

Our schemes simplified the fate of NH_3 captured by the canopy and assumed that such NH_3 is returned to the soil and becomes immediately accessible to plants, soil microbes, and bacteria, due to limited knowledge of the consequences of the canopy capturing process. A chamber study suggested that soybean can absorb up to 20 kg-N ha^{-1} of NH_3 via leaf capturing (Hutchinson et al., 1972), which is a significant amount compared to average fertilizer use for soybean of 25 kg-N ha^{-1} in previous versions of CLM. On the other hand, concentrated NH_3 could damage leaf tissues if the contacting plant fails to metabolize or detoxify such a reactive gas in time (Nemitz et al., 2001). The remaining captured NH_3 on the leaf surface can return to the soil via throughfall, but its magnitude is difficult to measure. These unspecified processes may induce uncertainties in our simulations, especially for plant growth and soil NH_4^+ content. This knowledge gap points to a demand for more field experiments to investigate the impacts of these processes.

FAO projects that fertilizer use will be increased by >30% (FAO, 2007) to boost food production to meet the fast-growing food demand by 2050. Such additional fertilizer injects mineral nitrogen into the soil that further fuels the volatilization of NH_3 spontaneously and hence promotes the subsequent formation of aerosol particles. This study shows the nonlinear

https://doi.org/10.5194/bg-2021-63
Preprint. Discussion started: 16 March 2021

impacts of nitrogen deposition and aerosol radiative effect on the environment. Thus, our work makes it possible to evaluate the intertwined consequences of such soaring use of fertilizer on NH_3 emission, atmospheric aerosols composition, and the corresponding aerosol-climate effect. Our results can provide scientific information to aid stakeholders in evaluating various global and regional plans for mitigating climate change and safeguarding a sustainable environment.

https://doi.org/10.5194/bg-2021-63
Preprint. Discussion started: 16 March 2021

Biogeosciences Discussions
Open Access
EGU

Appendix

A. Canopy Capture Fraction

Figure A1 shows the time series of the fractional amount of NH_3 captured by above-ground crop biomass. Our scheme showed that crops do not capture as much NH_3 as natural vegetation (~60–80% as estimated in our scheme) due to their smaller canopies, except for sugarcane and temperate soybean, which can retain >30% of NH_3 emitted. CLM5 allows crops to be irrigated or rainfed. We observed a general trend that irrigated crops retain more soil NH_3 emission than rainfed ones, which can be explained by their higher in-canopy air humidity. Despite instantaneous values varying with plant growth, our calculated canopy capture fractions are close to those used in previous studies (Bouwman et al., 1997), i.e., 20% for other shrubs, grasses, and crops.

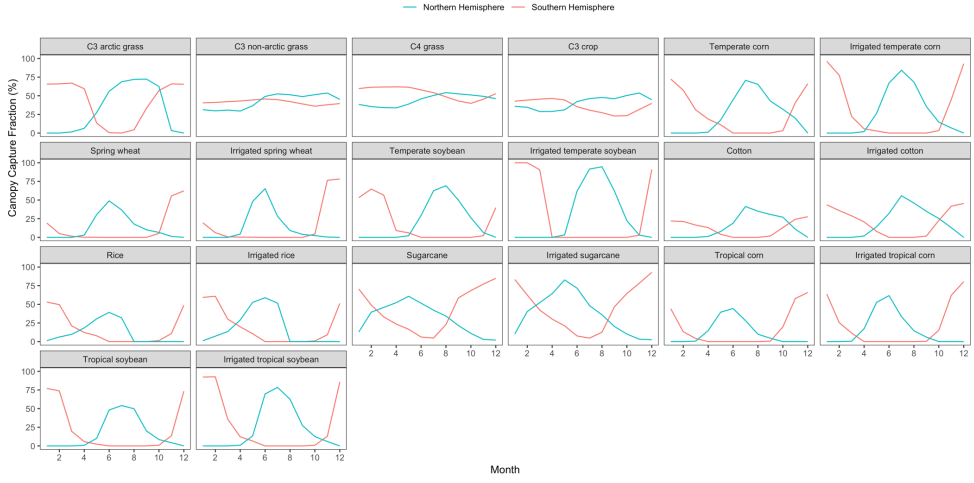

Figure A1. Monthly global-mean fractions of NH_3 captured (%) by each PFT canopy in each hemisphere.

https://doi.org/10.5194/bg-2021-63
Preprint. Discussion started: 16 March 2021

Table A1. Annual mean fraction of NH3 captured (%) by PFTs.

Crops	%NH_3 Captured
Temperate corn	24.8
Irrigated temperate corn	27.1
Spring wheat	12.7
Irrigated spring wheat	14.5
Temperate soybean	19.9
Irrigated temperate soybean	30.1
Cotton	13.2
Irrigated cotton	19.7
Rice	14.3
Irrigated rice	19.0
Sugarcane	37.2
Irrigated sugarcane	41.2
Tropical corn	14.5
Irrigated tropical corn	18.6
Tropical soybean	19.3
Irrigated tropical soybean	25.4

B. Sensitivity to Soil pH

CLM5 does not have a built-in method to compute soil pH implicitly. Thus, in **Results**, we used a constant global pH of 6.5, based on the implementation of the NH_3 volatilization scheme in DNDC (Li et al., 2012), to avoid the uncertain and highly spatial varying soil acidity. We tested the sensitivity of our simulated NH_3 emission by using the soil pH map from the Harmonized World Soil Database (HWSD) v1.2 (Wieder, 2014) showed in **Fig. B1(c)**. This soil pH dataset shows that the middle 50% of soil has pH values ranged from 5.4–7.0. When comparing maps in **Fig. B1(b)** and **(c)**, we observed that the more alkaline the soil is, the more soil emits NH_3. From our scheme (**Eq. (3)** in particular) for NH_3 volatilization, the emission rate is of the order of 10^{pH}:

$$\frac{\mathrm{d}[\mathrm{NH_3\,(g)}]}{\mathrm{d}t}_{\mathrm{soil}} \sim O\left(\frac{K_\mathrm{w}}{10^{-\mathrm{pH}}K_\mathrm{a}}\right) \sim O'(10^{\mathrm{pH}}) \quad \text{(B1)}$$

Figure B1(d) also illustrates and confirms this exponential relation between NH_3 emission and pH, pointing to a demand for an implicit approach for calculating prognostic soil alkalinity. Current version of CLM5 tracks only a few chemicals in soil, including NH_4^+, NO_3^-,

https://doi.org/10.5194/bg-2021-63
Preprint. Discussion started: 16 March 2021

and methane (CH_4), making the calculation of bulk soil pH difficult. Future models shall include crucial chemicals and processes, as characterized by experimental studies, that affect soil pH.

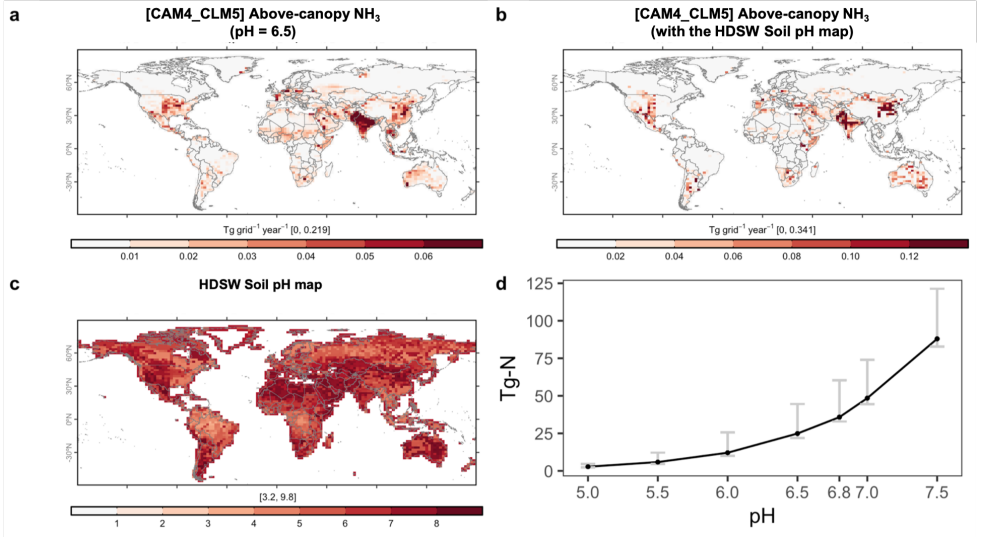

Figure B1. CLM5-simulated global soil NH_3 emission at above-canopy level with **(a)** a constant global pH of 6.5, and; **(b)** a spatially varying pH map re-gridded from the Harmonized World Soil Database v1.2 (HWSD) (Wieder, 2014), which is shown in map **(c)**. Graph **(d)** shows the total soil NH_3 emission against various global pH values from 5.0 to 7.5. Error bars indicate the maxima and minima across five years of simulation.

Code availability

The modified codes of CESM2 developed in this study will be available when this manuscript is accepted.

Author Contribution

All co-authors participated in designing the experiments. KMF and MVM developed the model code. KMF performed the simulations. KFM prepared the manuscript with contributions from all co-authors.

https://doi.org/10.5194/bg-2021-63
Preprint. Discussion started: 16 March 2021

Competing Interests

The authors declare that they have no conflict of interest.

Acknowledgments

This work was supported by the Research Grants Council (RGC) General Research Fund (Project #: 14323116) awarded to A. P. K. Tai. M. Val Martin acknowledges funding from the Leverhulme Trust through a Leverhulme Research Centre Award (RC-2015-029). We would also like to acknowledge the high-performance computing support from Cheyenne (doi:10.5065/D6RX99HX) provided by NCAR's Computational and Information Systems Laboratory, sponsored by the National Science Foundation.

References

Ansari, A. S. and Pandis, S. N.: Response of inorganic PM to precursor concentrations, 32, 2706–2714, https://doi.org/10.1021/es971130j, 1998.

Balasubramanian, S., Koloutsou-Vakakis, S., McFarland, D. M., and Rood, M. J.: Reconsidering emissions of ammonia from chemical fertilizer usage in midwest USA, 120, 6232–6246, https://doi.org/10.1002/2015JD023219, 2015.

Balasubramanian, S., Nelson, A., Koloutsou-Vakakis, S., Lin, J., Rood, M. J., Myles, L. T., and Bernacchi, C.: Evaluation of DeNitrification DeComposition model for estimating ammonia fluxes from chemical fertilizer application, 237–238, 123–134, https://doi.org/10.1016/j.agrformet.2017.02.006, 2017.

Beeckman, F., Motte, H., and Beeckman, T.: Nitrification in agricultural soils: impact, actors and mitigation, 50, 166–173, https://doi.org/10.1016/j.copbio.2018.01.014, 2018.

Behera, S. N. and Sharma, M.: Transformation of atmospheric ammonia and acid gases into components of PM2.5: An environmental chamber study, 19, 1187–1197, https://doi.org/10.1007/s11356-011-0635-9, 2012.

Bodirsky, B. L., Popp, A., Lotze-Campen, H., Dietrich, J. P., Rolinski, S., Weindl, I., Schmitz, C., Müller, C., Bonsch, M., Humpenöder, F., Biewald, A., and Stevanovic, M.: Reactive

https://doi.org/10.5194/bg-2021-63
Preprint. Discussion started: 16 March 2021

nitrogen requirements to feed the world in 2050 and potential to mitigate nitrogen pollution, 5, https://doi.org/10.1038/ncomms4858, 2014.

735 Bonan, G. B., Levis, S., Kergoat, L., and Oleson, K. W.: Landscapes as patches of plant functional types: An integrating concept for climate and ecosystem models, 16, 5-1-5–23, https://doi.org/10.1029/2000gb001360, 2002.

Bouwman, A. F., Lee, D. S., Asman, W. A. H., Dentener, F. J., Van Der Hoek, K. W., and Olivier, J. G. J.: A global high-resolution emission inventory for ammonia, 11, 561–587,
740 https://doi.org/10.1029/97GB02266, 1997.

Boylan, J. W. and Russell, A. G.: PM and light extinction model performance metrics, goals, and criteria for three-dimensional air quality models, 40, 4946–4959, https://doi.org/10.1016/j.atmosenv.2005.09.087, 2006.

Buijsman, E., Aben, J. M. M., Van Elzakker, B. G., and Mennen, M. G.: An automatic
745 atmospheric ammonia network in The Netherlands: Set-up and results, 32, 317–324, https://doi.org/10.1016/S1352-2310(97)00233-1, 1998.

Clarisse, L., Clerbaux, C., Dentener, F., Hurtmans, D., and Coheur, P. F.: Global ammonia distribution derived from infrared satellite observations, 2, 479–483, https://doi.org/10.1038/ngeo551, 2009.

750 Clarisse, L., Shephard, M. W., Dentener, F., Hurtmans, D., Cady-Pereira, K., Karagulian, F., Van Damme, M., Clerbaux, C., and Coheur, P. F.: Satellite monitoring of ammonia: A case study of the San Joaquin Valley, 115, 1–15, https://doi.org/10.1029/2009JD013291, 2010.

Crippa, M., Guizzardi, D., Muntean, M., Schaaf, E., Dentener, F., Van Aardenne, J. A., Monni, S., Doering, U., Olivier, J. G. J., Pagliari, V., and Janssens-Maenhout, G.: Gridded emissions
755 of air pollutants for the period 1970-2012 within EDGAR v4.3.2, 10, 1987–2013, https://doi.org/10.5194/essd-10-1987-2018, 2018.

Van Damme, M., Clarisse, L., Heald, C. L., Hurtmans, D., Ngadi, Y., Clerbaux, C., Dolman, A. J., Erisman, J. W., and Coheur, P. F.: Global distributions, time series and error characterization of atmospheric ammonia (NH3) from IASI satellite observations, 14, 2905–
760 2922, https://doi.org/10.5194/acp-14-2905-2014, 2014.

Van Damme, M., Whitburn, S., Clarisse, L., Clerbaux, C., Hurtmans, D., and Coheur, P. F.: Version 2 of the IASI NH3 neural network retrieval algorithm: Near-real-time and reanalysed datasets, 10, 4905–4914, https://doi.org/10.5194/amt-10-4905-2017, 2017.

Van Damme, M., Clarisse, L., Whitburn, S., Hadji-Lazaro, J., Hurtmans, D., Clerbaux, C., and
765 Coheur, P. F.: Industrial and agricultural ammonia point sources exposed, 564, 99–103, https://doi.org/10.1038/s41586-018-0747-1, 2018.

Davidson, E. A. and Trumbore, S. E.: Gas diffusivity and production of CO2 in deep soils of the eastern Amazon, 47, 550–565, https://doi.org/10.1034/j.1600-0889.47.issue5.3.x, 1995.

https://doi.org/10.5194/bg-2021-63
Preprint. Discussion started: 16 March 2021

Drewniak, B., Song, J., Prell, J., Kotamarthi, V. R., and Jacob, R.: Modeling agriculture in the Community Land Model, 6, 495–515, https://doi.org/10.5194/gmd-6-495-2013, 2013.

Emmons, L. K., Walters, S., Hess, P. G., Lamarque, J. F., Pfister, G. G., Fillmore, D., Granier, C., Guenther, A., Kinnison, D., Laepple, T., Orlando, J., Tie, X., Tyndall, G., Wiedinmyer, C., Baughcum, S. L., and Kloster, S.: Description and evaluation of the Model for Ozone and Related chemical Tracers, version 4 (MOZART-4), 3, 43–67, https://doi.org/10.5194/gmd-3-43-2010, 2010.

Erisman, J. W., Otjes, R., Hensen, A., Jongejan, P., Van Den Bulk, P., Khlystov, A., Möls, H., and Slanina, S.: Instrument development and application in studies and monitoring of ambient ammonia, Atmospheric Environment, 1913–1922 pp., https://doi.org/10.1016/S1352-2310(00)00544-6, 2001.

European Environment Agency: Ammonia (NH3) emissions, 2010.

European Environment Agency: EMEP/EEA air pollutant emission inventory guidebook 2013: Exhaust emissions from road transport, 160, https://doi.org/10.2800/92722, 2013.

Fagerli, H. and Aas, W.: Trends of nitrogen in air and precipitation: Model results and observations at EMEP sites in Europe, 1980-2003, 154, 448–461, https://doi.org/10.1016/j.envpol.2008.01.024, 2008.

Famulari, D., Fowler, D., Hargreaves, K., Milford, C., Nemitz, E., Sutton, M. A., and Weston, K.: Measuring eddy covariance fluxes of ammonia using tunable diode laser absorption spectroscopy, 4, 151–158, https://doi.org/10.1007/s11267-004-3025-1, 2004.

Fangmeierfl, A., Hadwiger-Fangmeierfl, A., Van Der Eerden, L., and J~iger, H.-J., Environmental Pollution, 43 pp., 1994.

FAO: Re-estimation of Global Fertilizer Requirement for 2015, 2030 and 2050, 2007.

Ferrara, R. M., Loubet, B., Di Tommasi, P., Bertolini, T., Magliulo, V., Cellier, P., Eugster, W., and Rana, G.: Eddy covariance measurement of ammonia fluxes: Comparison of high frequency correction methodologies, 158–159, 30–42, https://doi.org/10.1016/j.agrformet.2012.02.001, 2012.

Fowler, D., Pilegaard, K., Sutton, M. A., Ambus, P., Raivonen, M., Duyzer, J., Simpson, D., Fagerli, H., Fuzzi, S., Schjoerring, J. K., Granier, C., Neftel, A., Isaksen, I. S. A., Laj, P., Maione, M., Monks, P. S., Burkhardt, J., Daemmgen, U., Neirynck, J., Personne, E., Wichink-Kruit, R., Butterbach-Bahl, K., Flechard, C., Tuovinen, J. P., Coyle, M., Gerosa, G., Loubet, B., Altimir, N., Gruenhage, L., Ammann, C., Cieslik, S., Paoletti, E., Mikkelsen, T. N., Ro-Poulsen, H., Cellier, P., Cape, J. N., Horváth, L., Loreto, F., Niinemets, Ü., Palmer, P. I., Rinne, J., Misztal, P., Nemitz, E., Nilsson, D., Pryor, S., Gallagher, M. W., Vesala, T., Skiba, U., Brüggemann, N., Zechmeister-Boltenstern, S., Williams, J., O'Dowd, C., Facchini, M. C., de Leeuw, G., Flossman, A., Chaumerliac, N., and Erisman, J. W.: Atmospheric composition change: Ecosystems-Atmosphere interactions, https://doi.org/10.1016/j.atmosenv.2009.07.068, 2009.

https://doi.org/10.5194/bg-2021-63
Preprint. Discussion started: 16 March 2021

Del Grosso, S. J., Parton, W. J., Mosier, A. R., Ojima, D. S., Kulmala, A. E., and Phongpan, S.: General model for N2O and N2 gas emissions from soils due to dentrification, 14, 1045–1060, https://doi.org/10.1029/1999GB001225, 2000.

Gu, B. B. B., Ge, Y., Ren, Y., Xu, B., Luo, W., Jiang, H., Gu, B. B. B., and Chang, J.: Atmospheric Reactive Nitrogen in China: Sources, Recent Trends, and Damage Costs, 46, 9420–9427, https://doi.org/10.1021/es301446g, 2012.

Guenther, A. B., Jiang, X., Heald, C. L., Sakulyanontvittaya, T., Duhl, T., Emmons, L. K., and Wang, X.: The model of emissions of gases and aerosols from nature version 2.1 (MEGAN2.1): An extended and updated framework for modeling biogenic emissions, 5, 1471–1492, https://doi.org/10.5194/gmd-5-1471-2012, 2012.

Guthrie, S., Dunkerley, F., Tabaqchali, H., Harshfield, A., Ioppolo, B., and Manville, C.: Impact of ammonia emissions from agriculture on biodiversity: An evidence synthesis, https://doi.org/10.7249/rr2695, 2018.

Hoesly, R. M., Smith, S. J., Feng, L., Klimont, Z., Janssens-Maenhout, G., Pitkanen, T., Seibert, J. J., Vu, L., Andres, R. J., Bolt, R. M., Bond, T. C., Dawidowski, L., Kholod, N., Kurokawa, J., Li, M., Liu, L., Lu, Z., Moura, M. C. P., O'Rourke, P. R., and Zhang, Q.: Historical (1750–2014) anthropogenic emissions of reactive gases and aerosols from the Community Emissions Data System (CEDS), 11, 369–408, https://doi.org/10.5194/gmd-11-369-2018, 2018.

Van Hove, L. W. A., Koops, A. J., Adema, E. H., Vredenberg, W. J., and Pieters, G. A.: Analysis of the uptake of atmospheric ammonia by leaves of Phaseolus vulgaris L., 21, 1759–1763, https://doi.org/10.1016/0004-6981(87)90115-6, 1987.

Hu, J., Zhang, H., Ying, Q., Chen, S. H., Vandenberghe, F., and Kleeman, M. J.: Long-term particulate matter modeling for health effect studies in California - Part 1: Model performance on temporal and spatial variations, 15, 3445–3461, https://doi.org/10.5194/acp-15-3445-2015, 2015.

Huang, X., Song, Y., Li, M., Li, J., Huo, Q., Cai, X., Zhu, T., Hu, M., and Zhang, H.: A high-resolution ammonia emission inventory in China, 26, 1–14, https://doi.org/10.1029/2011GB004161, 2012.

Huijsmans, J. F. M., Vermeulen, G. D., Hol, J. M. G., and Goedhart, P. W.: A model for estimating seasonal trends of ammonia emission from cattle manure applied to grassland in the Netherlands, 173, 231–238, https://doi.org/10.1016/j.atmosenv.2017.10.050, 2018.

Hurrell, J. W., Holland, M. M., Gent, P. R., Ghan, S., Kay, J. E., Kushner, P. J., Lamarque, J.-F., Large, W. G., Lawrence, D., Lindsay, K., Lipscomb, W. H., Long, M. C., Mahowald, N., Marsh, D. R., Neale, R. B., Rasch, P., Vavrus, S., Vertenstein, M., Bader, D., Collins, W. D., Hack, J. J., Kiehl, J., and Marshall, S.: The Community Earth System Model: A Framework for Collaborative Research, 130204122247009, https://doi.org/10.1175/bams-d-12-00121, 2013.

https://doi.org/10.5194/bg-2021-63
Preprint. Discussion started: 16 March 2021

Hurtt, G. C., Chini, L. P., Frolking, S., Betts, R. A., Feddema, J., Fischer, G., Fisk, J. P., Hibbard, K., Houghton, R. A., Janetos, A., Jones, C. D., Kindermann, G., Kinoshita, T., Klein Goldewijk, K., Riahi, K., Shevliakova, E., Smith, S., Stehfest, E., Thomson, A., Thornton, P., van Vuuren, D. P., and Wang, Y. P.: Harmonization of land-use scenarios for the period 1500-2100: 600 years of global gridded annual land-use transitions, wood harvest, and resulting secondary lands, 109, 117–161, https://doi.org/10.1007/s10584-011-0153-2, 2011.

Hutchinson, G. L., Millington, R. J., and Peters, D. B.: Atmospheric Ammonia: Absorption by Plant Leaves, 175, 771–772, https://doi.org/10.1126/science.175.4023.771, 1972.

Ianniello, A., Spataro, F., Esposito, G., Allegrini, I., Hu, M., and Zhu, T.: Chemical characteristics of inorganic ammonium salts in PM2.5 in the atmosphere of Beijing (China), 11, 10803–10822, https://doi.org/10.5194/acp-11-10803-2011, 2011.

Institute for the Study of Earth, Oceans, and Space, University of New Hampshire: DNDC v9.5 Scientific Basis and Processes, 2017.

Krupa, S. V.: Effects of atmospheric ammonia (NH3) on terrestrial vegetation: A review, 124, 179–221, https://doi.org/10.1016/S0269-7491(02)00434-7, 2003.

Lamarque, J. F., Dentener, F., McConnell, J., Ro, C. U., Shaw, M., Vet, R., Bergmann, D., Cameron-Smith, P., Dalsoren, S., Doherty, R., Faluvegi, G., Ghan, S. J., Josse, B., Lee, Y. H., Mackenzie, I. A., Plummer, D., Shindell, D. T., Skeie, R. B., Stevenson, D. S., Strode, S., Zeng, G., Curran, M., Dahl-Jensen, D., Das, S., Fritzsche, D., and Nolan, M.: Multi-model mean nitrogen and sulfur deposition from the atmospheric chemistry and climate model intercomparison project (ACCMIP): Evaluation of historical and projected future changes, 13, 7997–8018, https://doi.org/10.5194/acp-13-7997-2013, 2013.

Lamarque, J.-F., Emmons, L. K., Hess, P. G., Kinnison, D. E., Tilmes, S., Vitt, F., Heald, C. L., Holland, E. A., Lauritzen, P. H., Neu, J., Orlando, J. J., Rasch, P. J., and Tyndall, G. K.: CAM-chem: description and evaluation of interactive atmospheric chemistry in the Community Earth System Model, 5, 369–411, https://doi.org/10.5194/gmd-5-369-2012, 2012.

Lawrence, D., Fisher, R., Koven, C., Oleson, K., Swenson, S., and Vertenstein, M.: Technical Description of version 5.0 of the Community Land Model (CLM), 337, 2020.

Lawrence, D. M., Fisher, R. A., Koven, C. D., Oleson, K. W., Swenson, S. C., Bonan, G., Collier, N., Ghimire, B., Kampenhout, L., Kennedy, D., Kluzek, E., Lawrence, P. J., Li, F., Li, H., Lombardozzi, D., Riley, W. J., Sacks, W. J., Shi, M., Vertenstein, M., Wieder, W. R., Xu, C., Ali, A. A., Badger, A. M., Bisht, G., Broeke, M., Brunke, M. A., Burns, S. P., Buzan, J., Clark, M., Craig, A., Dahlin, K., Drewniak, B., Fisher, J. B., Flanner, M., Fox, A. M., Gentine, P., Hoffman, F., Keppel-Aleks, G., Knox, R., Kumar, S., Lenaerts, J., Leung, L. R., Lipscomb, W. H., Lu, Y., Pandey, A., Pelletier, J. D., Perket, J., Randerson, J. T., Ricciuto, D. M., Sanderson, B. M., Slater, A., Subin, Z. M., Tang, J., Thomas, R. Q., Val Martin, M., and Zeng, X.: The Community Land Model Version 5: Description of New Features, Benchmarking, and Impact of Forcing Uncertainty, 11, 4245–4287, https://doi.org/10.1029/2018MS001583, 2019.

Lawrence, P. J. and Chase, T. N.: Representing a new MODIS consistent land surface in the Community Land Model (CLM 3.0), 112, https://doi.org/10.1029/2006JG000168, 2007.

https://doi.org/10.5194/bg-2021-63
Preprint. Discussion started: 16 March 2021

885 Leen, J. B., Yu, X. Y., Gupta, M., Baer, D. S., Hubbe, J. M., Kluzek, C. D., Tomlinson, J. M., and Hubbell, M. R.: Fast in situ airborne measurement of ammonia using a mid-infrared off-axis ICOS spectrometer, 47, 10446–10453, https://doi.org/10.1021/es401134u, 2013.

Levis, S., Badger, A., Drewniak, B., Nevison, C., and Ren, X.: CLMcrop yields and water requirements: avoided impacts by choosing RCP 4.5 over 8.5, 146, 501–515,
890 https://doi.org/10.1007/s10584-016-1654-9, 2018.

Li, C., Aber, J., Stange, F., Butterbach-Bahl, K., and Papen, H.: A process-oriented model of N 2 O and NO emissions from forest soils: 1. Model development, 105, 4369–4384, https://doi.org/10.1029/1999JD900949, 2000.

Li, C., Salas, W., Zhang, R., Krauter, C., Rotz, A., and Mitloehner, F.: Manure-DNDC: A
895 biogeochemical process model for quantifying greenhouse gas and ammonia emissions from livestock manure systems, 93, 163–200, https://doi.org/10.1007/s10705-012-9507-z, 2012.

Lin, B. Le, Sakoda, A., Shibasaki, R., and Suzuki, M.: A modelling approach to global nitrate leaching caused by anthropogenic fertilisation, Water Research, 1961–1968 pp., https://doi.org/10.1016/S0043-1354(00)00484-X, 2001.

900 Lu, X. K., Mo, J. M., and Dong, S. F.: Effects of nitrogen deposition on forest biodiversity: A review, Shengtai Xuebao/ Acta Ecologica Sinica, 5532–5548 pp., https://doi.org/10.1016/S1872-2032(09)60012-3, 2008.

National Oceanic and Atmospheric Administration: Atmospheric Ammonia: Sources and Fate - A Review of Ongoing Federal Research and Future Need, Journal of Molecular Liquids, 2000.

905 Nemitz, E., Milford, C., and Sutton, M. A.: A two-layer canopy compensation point model for describing bi-directional biosphere-atmosphere exchange of ammonia, 127, 815–833, https://doi.org/10.1256/smsqj.57305, 2001.

Neu, J. L. and Prather, M. J.: Toward a more physical representation of precipitation scavenging in global chemistry models: Cloud overlap and ice physics and their impact on
910 tropospheric ozone, 12, 3289–3310, https://doi.org/10.5194/acp-12-3289-2012, 2012.

Nevison, C., Hess, P., Riddick, S., and Ward, D.: Denitrification, leaching, and river nitrogen export in the Community Earth System Model, 8, 272–291, https://doi.org/10.1002/2015MS000573, 2016.

Norman, M. and Leck, C.: Distribution of marine boundary layer ammonia over the Atlantic
915 and Indian Oceans during the Aerosols99 cruise, 110, 1–11, https://doi.org/10.1029/2005JD005866, 2005.

Nowak, J. B., Neuman, J. A., Bahreini, R., Brock, C. A., Middlebrook, A. M., Wollny, A. G., Holloway, J. S., Peischl, J., Ryerson, T. B., and Fehsenfeld, F. C.: Airborne observations of ammonia and ammonium nitrate formation over Houston, Texas, 115, 22304,
920 https://doi.org/10.1029/2010JD014195, 2010.

https://doi.org/10.5194/bg-2021-63
Preprint. Discussion started: 16 March 2021

Parton, W. J., Holland, E. A., Del Grosso, S. J., Hartman, M. D., Martin, R. E., Mosier, A. R., Ojima, D. S., and Schimel, D. S.: Generalized model for NO $_x$ and N $_2$ O emissions from soils, 106, 17403–17419, https://doi.org/10.1029/2001JD900101, 2001.

Parton, W. J., Holland, E. A., Del Grosso, S. J., Hartman, M. D., Martin, R. E., Mosier, A. R., Ojima, D. S., and Schimel, D. S.: Generalized model for NO x and N 2 O emissions from soils , 106, 17403–17419, https://doi.org/10.1029/2001jd900101, 2004.

Paulot, F. and Jacob, D. J.: Hidden Cost of U.S. Agricultural Exports: Particulate Matter from Ammonia Emissions, 48, 903–908, https://doi.org/10.1021/es4034793, 2014.

Paulot, F., Jacob, D. J., Pinder, R. W., Bash, J. O., Travis, K., and Henze, D. K.: Ammonia emissions in the United States, European Union, and China derived by high-resolution inversion of ammonium wet deposition data: Interpretation with a new agricultural emissions inventory (MASAGE_NH3), 119, 4343–4364, https://doi.org/10.1002/2013JD021130, 2014.

Paulot, F., Jacob, D. J., Johnson, M. T., Bell, T. G., Baker, A. R., Keene, W. C., Lima, I. D., Doney, S. C., and Stock, C. A.: Global oceanic emission of ammonia: Constraints from seawater and atmospheric observations, 29, 1165–1178, https://doi.org/10.1002/2015GB005106, 2015.

Pleim, J. E., Bash, E. O., Walker, J. T., and Cooter, E. J.: Development and evaluation of an ammonia bidirectional flux parameterization for air quality models, 118, 3794–3806, https://doi.org/10.1002/jgrd.502622013, 2013.

Portmann, F. T., Siebert, S., and Döll, P.: MIRCA2000-Global monthly irrigated and rainfed crop areas around the year 2000: A new high-resolution data set for agricultural and hydrological modeling, 24, n/a-n/a, https://doi.org/10.1029/2008gb003435, 2010.

Puchalski, M. A., Sather, M. E., Walker, J. T., Lehmann, C. M. B., Gay, D. A., Mathew, J., and Robarge, W. P.: Passive ammonia monitoring in the United States: Comparing three different sampling devices, 13, 3156–3167, https://doi.org/10.1039/c1em10553a, 2011.

Riddick, S., Ward, D., Hess, P., Mahowald, N., Massad, R., and Holland, E.: Estimate of changes in agricultural terrestrial nitrogen pathways and ammonia emissions from 1850 to present in the Community Earth System Model, 13, 3397–3426, https://doi.org/10.5194/bg-13-3397-2016, 2016.

Saikawa, E., Schlosser, C. A., and Prinn, R. G.: Global modeling of soil nitrous oxide emissions from natural processes, 27, 972–989, https://doi.org/10.1002/gbc.20087, 2013.

Saikawa, E., Prinn, R. G., Dlugokencky, E., Ishijima, K., Dutton, G. S., Hall, B. D., Langenfelds, R., Tohjima, Y., Machida, T., Manizza, M., Rigby, M., O'Doherty, S., Patra, P. K., Harth, C. M., Weiss, R. F., Krummel, P. B., Van Der Schoot, M., Fraser, P. J., Steele, L. P., Aoki, S., Nakazawa, T., and Elkins, J. W.: Global and regional emissions estimates for N2O, 14, 4617–4641, https://doi.org/10.5194/acp-14-4617-2014, 2014.

https://doi.org/10.5194/bg-2021-63
Preprint. Discussion started: 16 March 2021

Shou, W., Zong, H., Ding, P., and Hou, L.: A modelling approach to assess the effects of atmospheric nitrogen deposition on the marine ecosystem in the Bohai Sea, China, 208, 36–48, https://doi.org/10.1016/j.ecss.2018.04.025, 2018.

Snider, G., Weagle, C. L., Murdymootoo, K. K., Ring, A., Ritchie, Y., Stone, E., Walsh, A., Akoshile, C., Anh, N. X., Balasubramanian, R., Brook, J., Qonitan, F. D., Dong, J., Griffith, D., He, K., Holben, B. N., Kahn, R., Lagrosas, N., Lestari, P., Ma, Z., Misra, A., Norford, L. K., Quel, E. J., Salam, A., Schichtel, B., Segev, L., Tripathi, S., Wang, C., Yu, C., Zhang, Q., Zhang, Y., Brauer, M., Cohen, A., Gibson, M. D., Liu, Y., Martins, J. V., Rudich, Y., and Martin, R. V.: Variation in global chemical composition of PM 2.5 : emerging results from SPARTAN, 16, 9629–9653, https://doi.org/10.5194/acp-16-9629-2016, 2016.

Sutton, M. A., Tang, Y. S., Dragosits, U., Fournier, N., Dore, A. J., Smith, R. I., Weston, K. J., and Fowler, D.: A Spatial Analysis of Atmospheric Ammonia and Ammonium in the U.K., 1, 275–286, https://doi.org/10.1100/tsw.2001.313, 2005.

Sutton, M. A., Erisman, J. W., Dentener, F., and Möller, D.: Ammonia in the environment: From ancient times to the present, 156, 583–604, https://doi.org/10.1016/j.envpol.2008.03.013, 2008.

Sutton, M. A., Reis, S., Riddick, S. N., Dragosits, U., Nemitz, E., Theobald, M. R., Tang, Y. S., Braban, C. F., Vieno, M., Dore, A. J., Mitchell, R. F., Wanless, S., Daunt, F., Fowler, D., Blackall, T. D., Milford, C., Flechard, C. R., Loubet, B., Massad, R., Cellier, P., Personne, E., Coheur, P. F., Clarisse, L., Van Damme, M., Ngadi, Y., Clerbaux, C., Skjøth, C. A., Geels, C., Hertel, O., Kruit, R. J. W., Pinder, R. W., Bash, J. O., Walker, J. T., Simpson, D., Horváth, L., Misselbrook, T. H., Bleeker, A., Dentener, F., and de Vries, W.: Towards a climate-dependent paradigm of ammonia emission and deposition, 368, https://doi.org/10.1098/rstb.2013.0166, 2013.

Tian, D. and Niu, S.: A global analysis of soil acidification caused by nitrogen addition, 10, https://doi.org/10.1088/1748-9326/10/2/024019, 2015.

Tie, X. and Cao, J.: Aerosol pollution in China: Present and future impact on environment, 7, 426–431, https://doi.org/10.1016/j.partic.2009.09.003, 2009.

US Environmental Protection Agency: National Emission Inventory (NEI) Report, 2014.

Vira, J., Hess, P., Melkonian, J., and Wieder, W. R.: An improved mechanistic model for ammonia volatilization in Earth system models: Flow of Agricultural Nitrogen version 2 (FANv2), Geosci. Model Dev., 13, 4459–4490, https://doi.org/10.5194/gmd-13-4459-2020, 2020.

Wang, J., Xing, J., Mathur, R., Pleim, J. E., Wang, S., Hogrefe, C., Gan, C. M., Wong, D. C., and Hao, J.: Historical trends in PM2.5-related premature mortality during 1990–2010 across the Northern Hemisphere, 125, 400–408, https://doi.org/10.1289/EHP298, 2017.

Wentworth, G. R., Murphy, J. G., Croft, B., Martin, R. V., Pierce, J. R., Côté, J. S., Courchesne, I., Tremblay, J. É., Gagnon, J., Thomas, J. L., Sharma, S., Toom-Sauntry, D., Chivulescu, A., Levasseur, M., and Abbatt, J. P. D.: Ammonia in the summertime Arctic marine boundary layer:

Sources, sinks, and implications, 16, 1937–1953, https://doi.org/10.5194/acp-16-1937-2016, 2016.

Wesely, M. L.: Parameterization of Surface Resistances to Gaseous Dry Deposition in Regional-Scale Numerical Models, 23, 1293–1304, https://doi.org/10.1016/j.atmosenv.2007.10.058, 1989.

Whitburn, S., Van Damme, M., Clarisse, L., Hurtmans, D., Clerbaux, C., and Coheur, P. F.: IASI-derived NH3 enhancement ratios relative to CO for the tropical biomass burning regions, 17, 12239–12252, https://doi.org/10.5194/acp-17-12239-2017, 2017.

Wieder, W.: Regridded Harmonized World Soil Database v1.2, https://doi.org/10.3334/ornldaac/1247, 2014.

Willem Asman; Mark A. Sutton: Ammonia : emission , atmospheric transport and deposition, 27–48, 1998.

Wortman, E., Tomaszewski, T., Waldner, P., Schleppi, P., Thimonier, A., Eugster, W., Buchmann, N., and Sievering, H.: Atmospheric nitrogen deposition and canopy retention influences on photosynthetic performance at two high nitrogen deposition Swiss forests, 64, 17216, https://doi.org/10.3402/tellusb.v64i0.17216, 2012.

Xing, Y. F., Xu, Y. H., Shi, M. H., and Lian, Y. X.: The impact of PM2.5 on the human respiratory system, https://doi.org/10.3978/j.issn.2072-1439.2016.01.19, 2016.

Xu, R. and Prentice, I. C.: Terrestrial nitrogen cycle simulation with a dynamic global vegetation model, 14, 1745–1764, https://doi.org/10.1111/j.1365-2486.2008.01625.x, 2008.

Yang, Y., Ruan, Z., Wang, X., Yang, Y., Mason, T. G., Lin, H., and Tian, L.: Short-term and long-term exposures to fine particulate matter constituents and health: A systematic review and meta-analysis, 247, 874–882, https://doi.org/10.1016/j.envpol.2018.12.060, 2019.

Zhang, J. and Liu, M. G.: Observations on nutrient elements and sulphate in atmospheric wet depositions over the northwest Pacific coastal oceans - Yellow Sea, 47, 173–189, https://doi.org/10.1016/0304-4203(94)90107-4, 1994.

Zhang, L., Chen, Y., Zhao, Y., Henze, D. K., Zhu, L., Song, Y., Paulot, F., Liu, X., Pan, Y., Lin, Y., and Huang, B.: Agricultural ammonia emissions in China: Reconciling bottom-up and top-down estimates, 18, 339–355, https://doi.org/10.5194/acp-18-339-2018, 2018.

Zhang, Y. and Niu, H.: The development of the DNDC plant growth sub-model and the application of DNDC in agriculture: A review, 230, 271–282, https://doi.org/10.1016/j.agee.2016.06.017, 2016.

Zhao, Y., Zhang, L., Tai, A. P. K., Chen, Y., and Pan, Y.: Responses of surface ozone air quality to anthropogenic nitrogen deposition in the Northern Hemisphere, 17, 9781–9796, https://doi.org/10.5194/acp-17-9781-2017, 2017.

https://doi.org/10.5194/bg-2021-63
Preprint. Discussion started: 16 March 2021

Zheng, Y., Xue, T., Zhang, Q., Geng, G., Tong, D., Li, X., and He, K.: Air quality improvements and health benefits from China's clean air action since 2013, 12, https://doi.org/10.1088/1748-9326/aa8a32, 2017.

Zöll, U., Brümmer, C., Schrader, F., Ammann, C., Ibrom, A., Flechard, C. R., Nelson, D. D., Zahniser, M., and Kutsch, W. L.: Surface-atmosphere exchange of ammonia over peatland using QCL-based eddy-covariance measurements and inferential modeling, 16, 11283–11299, https://doi.org/10.5194/acp-16-11283-2016, 2016.